

1 **Single-cell dissection of schizophrenia reveals neurodevelopmental-synaptic** 2 **axis and transcriptional resilience**

3 W. Brad Ruzicka^{1,2,3,5*}, Shahin Mohammadi^{3,4,5}, Jose Davila-Velderrain^{3,4}, Sivan Subburaju^{1,2}, Daniel Reed
4 Tso¹, Makayla Hourihan¹, & Manolis Kellis^{3,4*}

5 Author affiliations: ¹Laboratory for Epigenomics in Human Psychopathology, McLean Hospital, Belmont, MA,
6 USA, ²Harvard Medical School, Boston, MA, USA, ³Broad Institute of MIT and Harvard, Cambridge, MA, USA,
7 ⁴MIT Computer Science and Artificial Intelligence Laboratory, Cambridge, MA, USA, ⁵These authors
8 contributed equally: W. Brad Ruzicka, Shahin Mohammadi. *e-mail: wruzicka@mclean.harvard.edu;
9 manoli@mit.edu

10 **Abstract**

11 Schizophrenia is a devastating mental disorder with a high societal burden, complex pathophysiology, and
12 diverse genetic and environmental risk factors. Its complexity, polygenicity, and small-effect-size and cell-type-
13 specific contributors have hindered mechanistic elucidation and the search for new therapeutics. Here, we
14 present the first single-cell dissection of schizophrenia, across 500,000+ cells from 48 postmortem human
15 prefrontal cortex samples, including 24 schizophrenia cases and 24 controls. We annotate 20 cell types/states,
16 providing a high-resolution atlas of schizophrenia-altered genes and pathways in each. We find neurons are
17 the most affected cell type, with deep-layer cortico-cortical projection neurons and parvalbumin-expressing
18 inhibitory neurons showing significant transcriptional changes converging on genetically-implicated regions.
19 We discover a novel excitatory-neuron cell-state indicative of transcriptional resilience and enriched in
20 schizophrenia subjects with less-perturbed transcriptional signatures. We identify key trans-acting factors as
21 candidate drivers of observed transcriptional perturbations, including MEF2C, TCF4, SOX5, and SATB2, and
22 map their binding patterns in postmortem human neurons. These factors regulate distinct gene sets underlying
23 fetal neurodevelopment and adult synaptic function, bridging two leading models of schizophrenia
24 pathogenesis. Our results provide the most detailed map to date for mechanistic understanding and
25 therapeutic development in neuropsychiatric disorders.

26 **Introduction**

27 Schizophrenia afflicts young adults just as they approach their full potential, manifests as a combination of
28 psychosis, social withdrawal, and cognitive dysfunction, and often leads to a lifetime of profound and chronic
29 disability¹. Schizophrenia pathogenesis is thought to begin during neurodevelopment, yet symptoms do not
30 emerge until many years later in early adulthood². The complex etiology of schizophrenia is driven by both
31 genetic and environmental factors affecting a wide range of brain-related processes, including
32 neurodevelopment^{3,4}, cognition^{5,6}, synaptic function^{7,8}, neuronal excitability^{9,10}, and neuronal connectivity^{11,12}.

33 Decades-long efforts to decipher schizophrenia genetics have yielded 145+ robustly-associated genetic

34 loci^{13,14}, but their target genes and cell-types of action remain largely uncharacterized, hindering the search for
35 mechanistic insights and therapeutics development. Cell-type-specific profiles of reference (non-schizophrenia)
36 brain-sample transcriptomes have shown that genes near schizophrenia risk loci are expressed in pyramidal
37 neurons and specific subsets of inhibitory neurons¹⁵, but do not reveal whether schizophrenia-locus-proximal
38 genes are indeed differentially-expressed in schizophrenia, or whether increased or decreased expression is
39 risk-associated or protective. Conversely, schizophrenia case-control gene expression analyses using
40 homogenized cortical tissue have been carried out at the bulk level¹⁶⁻¹⁹, revealing several differentially-
41 expressed genes in schizophrenia. However, such bulk-level studies average gene expression across millions
42 of cells, merging together diverse and inconsistent cell types, and thus miss genes that are differentially-
43 expressed only in lower-abundance cell types and genes with opposite changes in different cell populations,
44 and can also result in false positives stemming from cell-type-composition changes between samples.
45 Emerging technologies for single-cell transcriptomics^{20,21} achieve both cell-type-specificity and reveal disease-
46 associated changes, as demonstrated for Alzheimer's Disease²², Autism Spectrum Disorder²³, Major
47 Depressive Disorder²⁴, and Multiple Sclerosis²⁵, but these have not been applied to schizophrenia to date.

48 Here, we present the first transcriptomic atlas of schizophrenia at single-cell resolution, profiling >500,000 cells
49 from postmortem human prefrontal cortex from 24 schizophrenia, and 24 age-matched control individuals. We
50 annotate 18 distinct cell types, including seven excitatory and six inhibitory neuronal subpopulations and five
51 non-neuronal cell types. We also identify a new excitatory neuron cell-state, Ex-SZTR, which is enriched for
52 differentially-expressed genes and significantly more prevalent in schizophrenia than in control individuals, but
53 surprisingly preferentially found in schizophrenia individuals with non-schizophrenia transcriptional signatures
54 across all other cell types, indicating transcriptional resilience. Schizophrenia-associated transcriptional
55 perturbations enrich in highly-specific cellular populations, including deep-layer cortico-cortical projection
56 neurons and PV-expressing inhibitory neurons, highlighting the importance of cell-type-specific assessments.
57 These changes preferentially perturb postsynaptic organization, synaptic plasticity, and neurodevelopmental
58 pathways, providing mechanistic insights into functional pathways that underlie schizophrenia perturbations.
59 Genes showing differential expression in schizophrenia are significantly enriched in the proximity of GWAS-
60 associated genes¹⁴ and linked to schizophrenia-associated genetic variants via enhancer-promoter loops in
61 adult dorsolateral prefrontal cortex²⁶, providing candidate target genes, the directionality of effect, and cell-
62 type-of-action for 68 of 145 schizophrenia loci. Searching for common upstream regulators for differentially-
63 expressed genes, we find that schizophrenia-associated transcriptional perturbations converge on a small
64 number of transcription factors, which are themselves encoded in schizophrenia-associated genetic loci,
65 including MEF2C, SATB2, SOX5, and TCF4. These factors act in both early fetal brain development and in
66 adult brain synaptic processes, thus linking two leading models of schizophrenia pathogenesis. Our results
67 provide both a unique resource for understanding the molecular biology of schizophrenia at single-cell
68 resolution, and numerous new insights for understanding candidate cell-type-specific driver genes, biological
69 pathways, master regulators, and resilience mechanisms, and for prioritizing target genes for therapeutic

70 development against this devastating disorder.

71 **Multiplexed single-cell profiling of schizophrenia**

72 To investigate schizophrenia-associated cell-type-specific transcriptional disruption within the complex
73 cytoarchitecture of the human brain, we used single-nucleus RNA sequencing (snRNA-seq) to profile
74 postmortem tissue samples from the prefrontal cortex (Brodmann Area 10) (**Fig. 1a**). We curated a cohort of
75 24 schizophrenia and 24 control subjects, balanced for gender (12 male and 12 female subjects per group),
76 age (ranging from 22 to 94 years, average 63.5 years), and postmortem interval (ranging from 6.9 to 26.3
77 hours, average 16.8 hours) (**Supplementary Table 1**). We reviewed medical records and incorporated
78 psychiatric medication exposures into our analysis to control for potential confounding effects of
79 pharmacotherapy. We multiplexed samples, pooling three schizophrenia and three control samples in each of
80 eight batches, using the Multiplexing Using Lipid Tagged Indices (MULTI-Seq)²⁷. Compared to standard
81 snRNA-seq protocols, sample multiplexing allows us to capture more cells from each individual while reducing
82 batch effects (by profiling both schizophrenia and control samples in the same sequencing library), reducing
83 the rate of undetected doublets (by using sample hashtags to remove cross-individual doublets), and lowering
84 sample preparation costs (by assessing more than one sample per 10x kit channel). After doublet removal, we
85 obtained 560,020 single-nucleus transcriptomes, including 266,431 cells from schizophrenia and 293,589 from
86 control individuals, profiled at an average depth of 12k cells per sample and 35k reads per cell
87 (**Supplementary Table 2**). We next removed genes expressed in less than ten cells in each batch, and cells
88 with fewer than 500 identified genes or more than 10% of unique molecular identifiers (UMIs) in mitochondrial
89 genes, resulting in 17,460 genes detected in 506,378 cells.

90 **Multiresolution dissection of cellular subpopulations**

91 We used our recently developed multiresolution cell-state discovery platform, ACTIONet²⁸, to identify both
92 discrete and continuous cell states (“archetypes”) using a coupled archetypal/network analysis. We first applied
93 ACTIONet to reconstruct the geometry of the cell-state landscape and used it to detect and remove outlier cells
94 that fall on the periphery of the constructed cell-cell similarity graph, keeping only the 386,065 highest-quality
95 cells with reproducible expression patterns. In the second round, we used the ACTIONet on the filtered cells
96 and identified 20 cell states in the combined population of schizophrenia and control subjects, nearly all of
97 which form dense clusters in the cell-cell similarity network (**Fig. 1b, Extended Data Fig. 1a**), with two notable
98 exceptions that we discuss below. Our 20 cell states captured all major cell types of the human prefrontal
99 cortex, including subtypes of excitatory and inhibitory neurons and glia (**Fig. 1b, d**). We verified these
100 annotations based on known marker gene expression patterns, by projecting individual marker genes on the
101 cell similarity network (**Fig. 1c**). *De novo* markers for these cell types are consistent with our previous studies
102 of the human prefrontal cortex²⁸ (**Supplementary Table 3**). Neuronal subtypes, particularly excitatory neurons,
103 showed higher numbers of expressed genes and identified UMIs (**Extended Data Fig. 2a, b**).

104 We also captured all major subtypes of GABAergic inhibitory neurons, including calcium-binding protein

105 parvalbumin (PV) expressing neurons, neuropeptide somatostatin (SST) neurons, and ionotropic serotonin
106 receptor 5HT3a (5HT3aR) neurons. Within these groups, we detected two PV-expressing subtypes of
107 inhibitory neurons (Basket and Chandelier), and two 5HT3aR-expressing subtypes (VIP+ and Reelin+), and
108 the recently-described Rosehip population²⁹. Cell groupings observed in the ACTIONet plot are consistent with
109 the developmental origin of cardinal interneuron subtypes (medial versus caudal ganglionic eminence),
110 demonstrating their shared transcriptional signatures³⁰.

111 Excitatory neurons exhibit a strong layer-specific pattern. We observed a consistent association of superficial-
112 layer excitatory neurons (layers II/III) with marker genes *CUX2* and *CBLN2*. However, intermediate and deep-
113 layer excitatory neurons are more intermixed, with layer IV/V neurons enriched for *RORB*, *FOXP2*, and
114 *RXFP1*, while deep layer neurons are marked with *TLE4*, *SEMA3E*, and *HTR2C* genes. Within the deep
115 cortical layers V and VI, we observe three distinct populations of excitatory neurons: cortico-fugal projection
116 neurons (Ex-L5/6) expressing *FEZF2*, and two distinct populations of cortico-cortical projection neurons (Ex-
117 L5/6-CCa, Ex-L5/6-CCb).

118 To further investigate differences between Ex-L5/6-CCa and Ex-L5/6-CCb, we focused on cells from control
119 individuals associated with these cell-types and performed differential expression analysis (Wilcoxon's rank-
120 sum test, **Supplementary Table 4**). We found that Ex-L5/6-CCa is enriched for genes involved in the
121 dopamine receptor signaling pathway, whereas Ex-L5/6-CCb is enriched for many key genes in glutamate
122 signaling. These distinct expression profiles point to physiological differences between two deep layer neuronal
123 populations likely related to specifics of their afferent and efferent connectivity with distinct cortical and
124 subcortical regions.

125 In addition to major cell types and their corresponding subtypes, we found two transcriptional archetypes that
126 capture continuous cell states shared across multiple subtypes of excitatory neurons. The first cross-cutting
127 cell state (Ex-NRGN) captures both a localized cell-type characterized by the expression of the *NRGN* gene
128 described in prior snRNA-seq studies of postmortem human brain²³, as well as a transcriptional signature
129 distributed among cells of different subtypes. The Ex-NRGN cell-state does not show enrichment for layer-
130 specific markers. In addition to *NRGN*, this population is marked by expression of the Brain Expressed and X-
131 Linked gene family members (*BEX1* and *BEX3*), calcium-binding enzymatic cofactor Calmodulin 3 (*CALM3*),
132 and *YWHAH*, which encodes a 14-3-3 signal transduction protein implicated in the conversion to the psychosis
133 of at-risk individuals³¹. Cells associated with the Ex-NRGN cell state highly express mitochondrial genes
134 (**Extended Data Fig. 2c**), an observation reproducible in an independent study²³ (**Extended Data Fig. 2d**).

135 The second cross-cutting cell-state (Ex-SZTR) is of particular interest, as it is preferentially associated with
136 excitatory neurons from schizophrenia patients (**Fig. 1e**). Ex-SZTR cells are enriched in superficial layer
137 excitatory neurons, as evidenced by the expression of layer-specific marker genes as well as the localization of
138 these cells within the cell network (**Fig. 1b,d, Extended Data Fig. 1a**). The top-ranked associated genes are

139 enriched for pathways related to synapse organization and synaptic plasticity, as well as neuronal process
140 morphology (**Supplementary Table 5**). We name this cell state Ex-SZTR for “schizophrenia transcriptional
141 resilience” as it is preferentially found in schizophrenia individuals whose transcriptional profiles are
142 surprisingly non-schizophrenia-like, as we discuss later in the text.

143 144 **Cell-type-specific schizophrenia-associated transcriptional perturbations**

145 Across all cell types/states, we identified a total of 1,637 up-regulated and 2,492 down-regulated differentially
146 expressed genes (DEGs) in schizophrenia (3,742 distinct schizophrenia-perturbed genes, as 387 genes are
147 both up- and down-regulated in distinct cell types), with the highest number of up-regulated genes in Ex-SZTR
148 and the highest number of downregulated genes observed in Ex-L5/6-CCb (**Fig. 2a, Supplementary Table 6**).
149 The majority of observed perturbations occur in neuronal populations, and ~60% of observed perturbations are
150 downregulation events. Among inhibitory neurons, PV-expressing subtypes (both Chandelier and Basket)
151 which have been the focus of much prior work³², indeed show the highest number of perturbed genes. Pairwise
152 comparison of the schizophrenia-associated transcriptional dysregulation between different cell subpopulations
153 reveals similarity in transcriptional changes within all neuronal subpopulations. Among neuronal cell types, we
154 observed a particularly high concordance of dysregulated genes among superficial layer excitatory neurons
155 (Ex-L2/3, Ex-L4, and Ex-L4/5) and Ex-L5/6-CCb (**Extended Data Fig. 3**).

156 To evaluate the reproducibility of our cell-type-specific dysregulated genes, we compared them to bulk-level
157 dysregulated genes across 559 schizophrenia and 936 control homogenized prefrontal cortex samples¹⁹. We
158 observed a significant overlap between the 2,450 upregulated (p -value $<10^{-8}$, Fisher’s exact test) and 2,371
159 downregulated (p -value $<10^{-29}$) bulk-level genes and the upregulated and downregulated gene sets identified
160 here, with downregulated genes in excitatory neurons having the strongest association (**Fig. 2a**). However,
161 among our cell-type-specific DEGs we identify novel genes not detected in prior tissue-level observations,
162 including genes in the Ex-SZTR cell state and subtypes of inhibitory neurons, highlighting the importance of
163 single-cell resolution analysis.

164 Among our DEGs (**Fig. 2b**), the transcriptional regulator *TCF4*¹⁴, which lies in a schizophrenia-associated
165 genetic locus, was the most widely-perturbed gene, upregulated in 14 of 20 cell types. Indeed, *TCF4* was also
166 detected as upregulated in bulk tissue RNA-Seq¹⁸. *TCF4* plays critical roles in both neurodevelopment and in
167 regulating the excitability of prefrontal cortex neurons³³, and was previously predicted as a “master regulator”
168 of schizophrenia gene network perturbations³⁴. Additionally, the molecular chaperone *CLU*, which also lies in a
169 schizophrenia-associated genetic locus¹⁴ and is most prominently expressed in astrocytes, was broadly
170 overexpressed across astrocytes, all excitatory neuron cell types, and most inhibitory neuron cell types.
171 Confirming our findings, *CLU* was previously recognized to be hypomethylated in schizophrenia bulk
172 postmortem brain samples³⁵, and overexpressed in laser-capture-microdissected excitatory neurons and in
173 parvalbumin-expressing inhibitory neurons^{36,37}. We also observed two gene families, neurexins (*NRXN1*,

174 *NRXN2*, *NRXN3*) and *SHANK* genes, to be commonly dysregulated across multiple neuronal subpopulations.
175 Neurexin genes serve as presynaptic cell-adhesion molecules and interact with neuroligins within the
176 postsynaptic membrane to mediate multiple aspects of synapse formation, structure, and function³⁸. In
177 contrast, *SHANK* genes encode postsynaptic scaffolding proteins essential for the organization of
178 glutamatergic synapses³⁹.

179 **Multi-gene transcriptional pathology score**

180 We next calculated a “transcriptional pathology score” (TPS) for each individual, based on the correlation of
181 their expression deviation (relative to the mean of all individuals) in each cell type, with the vector of
182 schizophrenia-associated differential expression in that cell type (**Fig. 2c, Extended Data Fig. 4,**
183 **Supplementary Table 7**). As expected, schizophrenia individuals showed significantly higher transcriptional
184 pathology scores than control individuals lying at opposite extremes of the TPS distribution, indicating
185 agreement between our predicted dysregulation scores and known phenotypic states. Individual CON7 was an
186 exception to this trend, showing schizophrenia-like expression profiles but lacking a schizophrenia diagnosis;
187 however, CON7 had a first-degree relative (his son) diagnosed with schizophrenia, suggesting a higher genetic
188 predisposition than expected possibly driven by a familial strong-effect genetic alteration. Surprisingly, we
189 found that TPS ranking was consistent across all neuronal cell types, rather than confined to the deep layer
190 excitatory and PV-expressing basket cell-types that showed the highest number of DEGs, indicating that global
191 pan-transcriptome gene-expression signatures of schizophrenia are robust across all neuronal cell-types (glial
192 cell types did not show such consistency).

193 Strikingly, schizophrenic individuals with an abundant subset of excitatory neurons in the Ex-SZTR cell state
194 showed among the lowest transcriptional pathology scores, even lower than most control individuals. In fact,
195 the two control individuals marked by the Ex-SZTR state show the two lowest schizophrenia transcriptional
196 pathology scores. This suggests that the presence of the Ex-SZTR cell state is correlated with “transcriptional
197 resilience”, whereby even schizophrenia cases show transcriptional profiles consistent with control individuals,
198 and control individuals show even more non-schizophrenia-like transcriptional signatures. We do not find the
199 Ex-SZTR cell-state to be associated with exposure to specific medications or levels of exposure to
200 pharmacologic classes. Instead, we interpret it as a potential mechanism of transcriptional compensation or
201 resilience to schizophrenia at the molecular level worthy of further investigation.

202 **Experimental validation of differentially expressed genes**

203 We next used fluorescence *in situ* hybridization (RNAscope) to experimentally validate both the cell-type-
204 specific expression and the differential expression of four differentially-expressed genes across six individuals.
205 We selected two upregulated genes (*TCF4*, *CLU*) and two down-regulated genes (*SHANK2*, *UNC13A*), which
206 showed strong and consistent changes across the majority of neuronal cell-types, and validated them in two
207 schizophrenia, two control, and two transcriptionally-resilient schizophrenia individuals. The resulting images

(Fig. 2d, Extended Data Fig. 5) show clear localization of these transcripts in excitatory neurons of the superficial cortical layers (*CUX2* staining). Quantification of transcript abundance (using dotdotdot⁴⁰) confirmed the highest expression for schizophrenia individuals, a lower expression for control individuals, and the lowest expression for transcriptionally-resilient individuals for *TCF4* and *CLU*, and the opposite trend for *SHANK2* and *UNC13A*, strongly confirming the cell-type-specificity, differential expression, and directionality of our findings, and also confirming the surprising behavior of transcriptionally-resilient individuals.

Dysregulated genes converge on synaptic plasticity, organization, and development

Observed gene expression changes suggest that schizophrenia predominantly impacts the transcriptional state of neuronal populations. To investigate whether neuronal processes are consistently dysregulated, or, alternatively, diverse neuronal functions are perturbed across cell subpopulations more specifically, we designed and performed extensive pathway enrichment analyses. We curated and organized relevant biological pathways into 14 neuronally-associated functional categories within three major themes with direct relevance to the etiology of schizophrenia: synaptic organization⁴¹, synaptic plasticity², and neurodevelopment⁴² (**Supplementary Table 8a**). We observe a pan-neuronal overrepresentation of pathways related to post-synaptic processes within both up- and downregulated genes, consistent with genetic and proteomic evidence that schizophrenia perturbations converge on the postsynaptic density^{43,44}.

Neurodevelopmental pathways show higher enrichment among upregulated genes, whereas glutamate signaling and synaptic plasticity are dominantly downregulated in schizophrenia. Among subpopulations of inhibitory neurons, PV- and SST-expressing neurons show the most robust functional enrichment with up- and downregulated genes, respectively (**Fig. 2e, Supplementary Table 8b,c**).

In addition to these major categories, we identified the disruption of cytoskeletal processes to be specifically enriched in the Ex-SZTR cell-state. This includes differential expression of genes involved in lamellipodium organization and assembly, migration (*CAPZB*, *CARMIL1*, *SLIT2*), morphologic regulation of axons, dendrites, and dendritic spines (*CARMIL1*, *GOLPH3*, *SRGAP2*, *VAV2*⁴⁵, *VAV3*, *WASF3*⁴⁶), and axon guidance (*ABLIM1*, *NCK1*⁴⁷, *PTPRO*, *SLIT2*). These findings in the Ex-SZTR cell-state, which is predominantly associated with markers of the superficial cortical layers, are consistent with previous studies describing aberrant pyramidal cell density and morphology predominantly within layers II and III⁴⁸⁻⁵⁰.

Correlated patterns of genetic and cell-type-specific expression perturbations

Seeking insights into the association between transcriptional alterations and schizophrenia manifestation, we investigated the relationship between dysregulated genes and genetic risk factors. By assessing the cell-type-specific differential expression of genes within 145 genomic loci significantly associated with schizophrenia¹⁴, we discovered significant differential expression events in at least one cell type within 68 of these loci (**Fig. 3a, Supplementary Table 9**). These novel associations identify putative causal mechanisms for more schizophrenia risk loci than previously possible using bulk tissue gene expression data, explaining the

242 functional relevance of these loci with candidate genes, cell-type of action, and direction of effect.

243 The majority of schizophrenia DEGs providing explanation for these 68 genomic loci were maximally perturbed
244 in excitatory neuronal populations, while 13 were most robustly altered in inhibitory neurons, and two genes in
245 astrocytes and two in oligodendrocytes. Perturbation of explanatory genes within these regions was split nearly
246 equally between up and downregulation (32 up vs. 36 down). Many explanatory genes were dysregulated in a
247 small number or only a single cell-type, or dysregulated in opposing directions across multiple cell-types,
248 resulting in their not being identified as schizophrenia DEGs in prior studies of bulk tissue. For example, the
249 *CALB2* gene encodes the calcium binding protein calretinin which is expressed specifically in In-VIP and In-
250 SST populations and contributes to long-term potentiation through regulation of neuronal excitability⁵¹, and
251 *CALB2* was specifically upregulated in only the In-VIP cell-type. *ALMS1* encodes a microtubule organizing
252 protein, and this gene was downregulated specifically in PV-expressing interneurons. Similarly, we found
253 multiple GWAS explanatory genes that were specifically dysregulated in the Ex-SZTR cell-type (*CPEB1*,
254 *GPR135*, *ZNF804A*), or upregulated in Ex-SZTR but downregulated across other populations (*BCL11B*,
255 *RALGAPA2*).

256 In addition to schizophrenia¹⁴, we further considered four psychiatric disorders that are known to share genetic
257 risk factors⁵²: major depressive disorder (MDD)⁵³, bipolar disorder (BD)⁵⁴, autism spectrum disorder (ASD)⁵⁵,
258 and attention-deficit/hyperactivity disorder (ADHD)⁵⁶. This approach allows us to distinguish schizophrenia from
259 general psychiatric illness-related associations. As a point of contrast, we included Alzheimer's disease (AD)⁵⁷,
260 a neurodegenerative disorder not expected to be genetically related to schizophrenia. For each gene/trait pair,
261 we computed an aggregate genetic perturbation score using H-MAGMA⁵², a tool that associates GWAS risk
262 variants to genes based on proximity to gene bodies, promoter regions, or regions linked to genes through
263 chromatin looping. We only considered evidence of distal regulatory links occurring in the adult dorsolateral
264 prefrontal cortex²⁶. As a measure of transcriptional perturbation for schizophrenia, we used the absolute value
265 of the t-statistics computed in the cell-type-specific differential expression analysis.

266 Correlation analysis between genetic and transcriptional perturbation scores for schizophrenia uncovered a
267 strong association within neuronal subpopulations, suggesting a substantial causal effect for observed
268 transcriptional alterations (**Fig. 3b**). We found that many of the cell-types whose transcriptional perturbations
269 show a strong association with schizophrenia genetic risk variants are also associated with risk variants for
270 bipolar and major depressive disorders, which is consistent with their previously-reported strong genetic
271 relationships both at the level of genetic correlations and gene-level overlaps⁵². We found weaker relationships
272 between schizophrenia transcriptional perturbations and ASD risk^{52,58}, consistent with the known lower
273 correlation of genetic risk between these disorders⁵⁸. Indeed, schizophrenia transcriptional perturbations
274 showed overlap with genetic risk loci for all neuropsychiatric disorders we assessed, while as expected we
275 found no overlap with genetic risk for the neurodegenerative disorder AD.

276 Across excitatory neuronal subpopulations, the relation between transcriptional and genetic perturbation was
277 strongest for the Ex-SZTR cell state, followed by deep-layer corticocortical projection neurons. The Ex-SZTR
278 cell state is predominantly associated with superficial-layer excitatory neurons (layers II/III), whereas cortico-
279 cortical excitatory neurons are enriched for layer V. The observed layer-specificity of perturbations is consistent
280 with the enrichment of schizophrenia genetic variants proximal to genes preferentially expressed in layer II and
281 layer V⁵⁹. Among inhibitory neurons, we detected the strongest association between schizophrenia DEGs and
282 genomic variants in In-PV-Basket cells, consistent with the known dysregulation of PV-expressing GABAergic
283 neurons in schizophrenia hypothesized to contribute to the disruption of synchronous neural activity in
284 schizophrenia^{60,61}. Unlike neuronal populations, we did not observe any significant association between
285 patterns of differential expression and genetic association in either glial or endothelial cells, suggesting non-
286 neuronal cell types do not play a primary role in schizophrenia pathologies mediated by transcriptional
287 dysregulation.

288 We next examined genes that show both genetic and transcriptional perturbations, focusing on the cell-types
289 most enriched for schizophrenia DEGs (Ex-SZTR, deep-layer cortico-cortical excitatory neurons, and In-PV-
290 Basket cells, **Fig. 3c, Extended Data Fig. 6**). Among these genes we found *TCF4*, a regulator of pyramidal
291 cell excitability whose target genes are also schizophrenia-associated and cluster in neurodevelopmental
292 pathways⁶²; *CLIP1*, a linker protein involved in microtubule trafficking of cargo within axons and dendrites⁶³;
293 *CACNA1C*, an ion channel with key roles in synaptic plasticity and neurodevelopment; *ZKSCAN3*, a
294 transcription factor implicated in autophagy; and *PGBD1*, a transposase with brain-specific expression and
295 unknown functionality.

296 **Transcriptional dissection of trans-acting factors reveals common regulators**

297 While individual DEGs may be affected by *cis*-acting genetic variants, coordinated expression changes are
298 often driven by common upstream transcriptional regulators⁶⁴. To prioritize such potential factors, we ranked a
299 total of **1,632** transcription factors (TFs), based on the degree to which their putative target genes overlap with
300 schizophrenia DEGs⁶⁵ (**Supplementary Table 10**). From this data, we identified, for each cell type, a list of
301 candidate regulators and tested whether their functional annotations converge to similar pathways as those
302 observed for DEGs (**Fig. 2c**). Surprisingly, TFs were strongly enriched only in neurodevelopmental pathways
303 (**Fig. 4a, Supplementary Table 11**), and not in synaptic function or signaling pathways.

304 To assess the association of schizophrenia genetic risk loci with transcriptional regulators in addition to
305 downstream transcriptional dysregulation directly, we focused on a subset of GWAS-associated TFs targeting
306 DEGs. We identified a set of seven such factors (*TCF4*, *SATB2*, *MEF2C*, *FOXP1*, *SOX5*, *ZNF536*, and
307 *ZNF804A*) with very strong overlap between their putative target genes and schizophrenia DEGs across all
308 neuronal cell-types/states (**Extended Data Fig. 7**). Interestingly, these TFs again point to neurodevelopmental
309 functions. *TCF4* is a broadly expressed helix-loop-helix transcription factor involved in nervous system
310 development that, when disrupted, causes the severe neurodevelopmental disorder Pitt Hopkins Syndrome;

SOX5 is implicated in fate determination and regulation of corticofugal projection neuron development, with loss-of-function perturbations leading to disrupted neuronal proportions and emergence timing⁶⁶; ZNF804A is involved in neurodevelopment, neuronal migration, and protein translation. To test whether additional neurodevelopmentally-associated transcriptional regulators not implicated by schizophrenia genetic studies might be functionally relevant in the context of schizophrenia by sharing converging behavior with these lead factors, we used the set of top-ranked TFs that are also annotated with neurodevelopmental functions to identify modules of coherent TFs. We constructed a TF-TF co-expression network and applied a clustering algorithm to identify five neurodevelopmentally-related, schizophrenia-associated TF modules (**Fig. 4b**, **Supplementary Table 12, 13**). In addition to the lead GWAS-associated factors, we found additional factors with known neurodevelopmental roles, including TBR1, which interacts with a SOX5/SATB2 circuit thought to regulate layer specification during fetal neurogenesis⁶⁷.

Among these modules, we found a TF group highly enriched for both schizophrenia- and neurodevelopmental delay (NDD)-associated genetic variants (**schizophrenia** p -value: 1.2×10^{-7} , **NDD** p -value: 3×10^{-6} , Fisher's exact test). NDD encompasses a broad category of disorders characterized by disrupted development of the nervous system leading to abnormal brain function, including intellectual disability, movement, speech, and tic disorders⁶⁸. We observed a significant overlap between genetically-identified NDD-associated TFs (de novo mutations and CNVs)⁶⁹ and our top-ranked schizophrenia TFs, in particular, TFs mediating upregulated genes in Ex-SZTR and Ex-NRGN, as well as downregulated genes across multiple subtypes of excitatory neurons (**Extended Data Fig. 8**). We observed a significant over-representation of the schizophrenia-GWAS associated TFs among the top-10 ranked TFs (lead NDD TFs), where NDD-associated factors are sorted based on their overall ChEA score (p -value $< 7 \times 10^{-7}$, Fisher's exact test). The majority of the lead NDD TFs (7/10) are also involved in neurodevelopment (**Extended Data Fig. 9**). Thus, we identified a group of coregulated TFs that are associated with (1) downstream schizophrenia-associated transcriptional dysregulation in neurons of the adult cortex, (2) schizophrenia genetic risk, and (3) genetic risk for disrupted neurodevelopment.

Two of the modules identified herein are consistent with neurodevelopmentally-associated gene modules recently reported by the PsychENCODE Consortium (PEC)⁷⁰. GWAS-enriched modules MEF2C/SATB2 and ZNF804A/ZEB2 strongly map to modules ME37 and ME32 in the PEC dataset, both of which were also reported to be enriched for schizophrenia variants. The latter module contains 19 TFs, 9 of which overlap with the MEF2C/SATB2 module (adjusted p -value $< 10^{-10}$, Fisher's exact test). The overlap covers the majority of GWAS-associated TFs, including SOX5, SATB2, MEF2C, TCF4, and EMX1 (**Fig. 4c**).

Experimentally validated TF targets confirm developmental-synaptic axis

To further investigate the link between the prioritized TFs and schizophrenia DEGs, we next tested whether active cis-regulatory elements that are targeted by these TFs show preferential association with schizophrenia DEGs. To this end, we performed Cleavage Under Targets and Tagmentation (CUT&Tag⁷¹) assays to map the

346 binding of MEF2C, SATB2, SOX5, and TCF4 genome-wide in neuronal nuclei sampled from four
347 schizophrenia and four control individuals within our larger cohort. For each transcription factor, we defined a
348 master-set of targeted regions that are identified in at least one sample. These master-sets of regulatory
349 elements were then projected onto the set of regulatory elements defined by the PEC developing human brain
350 dataset⁷⁰, which is a union of enhancers/promoters across different stages of brain development (**Extended**
351 **Data Fig. 10**). Finally, we mapped these TF-centric active regulatory elements to their putative target genes,
352 considering both proximal and distal interactions.

353 Given the set of target genes for each of these factors, we performed functional enrichment analysis to
354 uncover the neuronally-associated categories that are related to each TF's targets (**Fig. 5a**). Observed targets
355 of these TFs show a functional enrichment profile highly similar to that of up- and downregulated schizophrenia
356 DEGs (**Fig. 2e**), with prominent enrichment in categories related to postsynaptic and neurodevelopmental
357 processes, supporting a functional role for these TFs in dysregulation of these events in schizophrenia.

358 We then assessed the overlap of target genes with up- and downregulated schizophrenia DEGs independently
359 (**Fig. 5b**). We found a high degree of overlap between identified target genes and schizophrenia DEGs across
360 a wide-range of excitatory neurons, with the largest overlap between TF targeted genes and Ex-L4/5
361 upregulated and EX-L5/6-CCb downregulated DEGs. Among inhibitory neuronal populations, PV and SST
362 expression subtypes which originate in the medial ganglionic eminence showed markedly stronger
363 associations than inhibitory neurons originating in the caudal ganglionic eminence (In-Reelin, In-Rosehip, and
364 In-VIP). Finally, we did not observe a strong association between identified target genes and DEGs in non-
365 neuronal cell-types.

366 Target genes for SOX5 and SATB2, which play prominent roles in early neurodevelopment, exhibit a higher
367 degree of overlap with upregulated genes than MEF2C or TCF4. Conversely, SOX5 has an insignificant
368 association with downregulated genes, whereas MEF2C shows the strongest association with downregulated
369 genes, consistent with MEF2C's role as a transcriptional repressor⁷². This suggestion of up and downregulated
370 schizophrenia DEGs having distinct associations with neurodevelopmental stages prompted us to investigate
371 how the regulatory landscape of schizophrenia DEGs varies across brain development. We identified cis-
372 regulatory elements associated with different stages of brain development based on H3K27ac-enriched
373 genomic regions profiled in the human brain by the PEC⁷⁰, and linked enhancers with genes using evidence of
374 physical chromatin interaction (HiC profiles) and genomic proximity. Associating fetal and adult regulatory
375 elements independently with schizophrenia DEGs, we found that upregulated genes are predominantly linked
376 to enhancers that are specific to the fetal stage, whereas downregulated genes are linked to enhancers that
377 are either shared between the fetal and adult brain or are unique to the adult brain (**Fig. 5c**). Among the
378 strongest connections, we found Ex-SZTR upregulated and Ex-L5/6-CCb downregulated genes to be
379 associated with shared enhancers, while Ex-L4/5 upregulated genes are enriched for fetal-specific enhancers.

380 **Discussion**

381 In this work, we presented the first single-cell transcriptomic case-control dissection of schizophrenia,
382 producing an invaluable high-resolution and high-quality dataset of more than 500,000 single-cell
383 transcriptomes. We annotated 18 neuronal and glial cell types and two excitatory-neuron cross-cutting cellular
384 states, which we used to investigate cell-type-specific schizophrenia-dysregulated genes, pathways, and
385 regulators. The vast majority of differentially-expressed genes were cell-type-specific and undetectable in bulk
386 datasets, including 387 genes that were both upregulated and downregulated in distinct cell populations,
387 highlighting the importance of our single-cell datasets.

388 Within neuronal subpopulations, we uncovered both wide-spread and subtype-specific transcriptional changes
389 in both glutamatergic and GABAergic neurons, in particular PV-expressing interneurons, that are not readily
390 detectable in bulk tissue. Our results reveal the central role in schizophrenia for genes and regulators involved
391 in synapse formation/structure/function, with synaptic dysregulation of different neuronal subtypes implicating
392 distinct but functionally-related genes. Unexpectedly, the transcription factors targeting these synapse-related
393 genes enrich primarily neurodevelopmental processes, linking disruption of early neurodevelopment and adult
394 synaptic dysfunction and providing a novel bridge between two prominent theories of schizophrenia
395 pathogenesis. Furthermore, across multiple neuronal populations, upregulated genes implicated fetal
396 enhancers while downregulated genes implicated adult enhancers, suggesting impairment of epigenomic
397 differentiation of brain-specific enhancers across development as an underlying mechanistic paradigm.

398 Cutting across multiple subtypes of excitatory neurons within multiple layers, we uncovered a new cellular
399 state, Ex-SZTR, overrepresented in schizophrenic individuals but surprisingly associated with transcriptional
400 signatures of non-schizophrenia individuals across all other neuronal cell types, indicative of transcriptional
401 resilience. This relationship between gene-regulatory changes in only one cellular sub-state and global
402 transcriptional dysregulation in other neuronal cell types is reminiscent of the role of PV-expressing inhibitory
403 neurons in regulating synchronous firing of assemblies of excitatory neurons, a process implicated in multiple
404 neurodegenerative and psychiatric disorders^{73,74}. Indeed, we found that PV interneurons showed the strongest
405 correlation with non-schizophrenia (“resilience”) transcriptional signatures for the most transcriptionally-resilient
406 individuals, suggesting a potential interplay between Ex-SZTR and PV-expressing interneurons. While the
407 genetic and environmental factors influencing the Ex-SZTR cell state require further investigation, these
408 tantalizing findings suggest a new potential mechanism of resilience to schizophrenia molecular pathologies
409 that may be exploitable for new whole-brain therapeutic interventions against schizophrenia.

410 Our cell-type-specific DEGs showed a highly-significant enrichment in genetic loci associated with
411 schizophrenia, with schizophrenia-differentially-expressed genes in approximately half of all schizophrenia
412 GWAS loci¹⁴, including many loci previously lacking any mechanistic hypothesis. This substantial overlap
413 suggests potential mediating roles of these genes in linking genetic causation and molecular phenotypic

414 manifestation and helps reveal putative target genes that may be mediating the genetic effects of these loci,
415 the cell type in which these genes may be acting, and the directionality of their effect to distinguish protective
416 vs. risk-increasing gene expression changes. These insights can be invaluable in guiding the development of
417 therapeutic interventions, deciding on genes to target, the cell types in which to observe their impact, and
418 whether pharmaceutical interventions should be inhibitory or inducing, especially given the greatly-increased
419 success of therapeutic efforts with genetic support⁷⁵. Across GWAS loci, deep-layer excitatory neurons,
420 cortico-cortical projection neurons, and PV-expressing basket interneurons showed the strongest enrichments,
421 indicating central roles in mediating causal genetic effects. These enrichments between our differentially-
422 expressed genes and GWAS loci held across multiple psychiatric disorders, consistent with the shared
423 heritability between them⁵⁸, but were absent from Alzheimer's GWAS loci, providing confidence about the
424 specificity of our analyses.

425 These high-resolution cell-type-specific dysregulated gene sets also enabled insights into the upstream
426 transcription factors (TFs) most likely to influence these changes. Unlike dysregulated genes, these factors are
427 predominantly enriched for neurodevelopmental pathways. In particular, multiple lines of evidence reveal a
428 central role for four master regulators, namely TCF4, MEF2C, SOX5, and SATB2, which: (1) regulate
429 schizophrenia dysregulated genes primarily in neurons; (2) are genetically associated with both schizophrenia
430 and NDD; and (3) are key neurodevelopmental regulatory factors⁷⁰. We experimentally validated that the target
431 genes of these factors are schizophrenia DEGs, confirming their relevance to schizophrenia pathology.
432 Because these TFs are major regulators of neurodevelopment with strong evidence for their action as
433 upstream regulators of neuronal schizophrenia DEGs in adult synaptic function, we propose that their
434 pleiotropic roles may represent a link between early neurodevelopmental disruptions and adult brain function.
435 How genetic or early environmental perturbations to these TFs impact function to increase the risk for
436 schizophrenia, and why it is only later in life that the phenotypic effects manifest, cannot be answered at
437 present. However, our observations open up opportunities for future mechanistic studies tracking the
438 developmental consequences of direct genetic perturbations to the candidate schizophrenia regulators and
439 target genes put forward here.

440 While providing numerous biological insights, we acknowledge that the scope of this work is limited by current
441 technologies. As is necessary for investigating postmortem brain tissue, we measured transcriptomes of
442 isolated single-nuclei, and the differences between nuclear and whole-tissue RNA content must be considered
443 in the interpretation of this work. Additionally, there are many mechanisms critical to brain function not visible to
444 this methodology, such as mRNA splicing or trafficking of resident dendritic mRNAs. Another technical
445 limitation of this work is the inability to spatially resolve differential expression events, and we have addressed
446 this problem computationally and histologically where possible. These technology-specific limitations provide
447 an opportunity for future research when newer, more advanced technologies are routinely available.
448 Additionally, while our case-control design is a strength of the study, this focus on patient tissue does not allow

449 experimental manipulation to investigate the causality of our validated observations, and experiments in model
450 systems are needed. Individuals with schizophrenia have very diverse experiences of treatment and clinical
451 outcomes. Our study design is well powered for comparison of schizophrenia vs. control, but identification of
452 trends within subgroups of schizophrenia subjects affected by specific environmental, genetic, and treatment
453 factors will require larger numbers of subjects.

454 This work utilized a rigorous study design and analysis plan to address potential confounds that are common to
455 investigations of postmortem human brain tissue. Through balanced inclusion of schizophrenia and control
456 subjects in each multiplexed sample preparation and sequencing library, we observed a remarkably low batch
457 effect in our data, and almost no doublet contamination, two common problems with microfluidics-based
458 snRNA-seq. We balanced diagnostic groups for demographic variables, including age, gender, and
459 postmortem interval, and also controlled for these variables by including them as covariates in our analyses.
460 We also controlled for psychiatric medications by including them as quantitative covariates in our analysis, as
461 nearly all chronic schizophrenia patients receive longstanding pharmacologic treatment while individuals
462 without psychiatric illness do not, and thus psychiatric diagnostic groups are not easily balanced for psychiatric
463 medication exposures.

464 The data presented here offer a cell-type-specific reframing of schizophrenia transcriptional pathology by
465 revealing specific cell populations impacted by schizophrenia genes, variants, and regulators. Identification of
466 pleiotropic transcriptional regulators linking developmental and adult schizophrenia-associated pathologies,
467 and the newly discovered transcriptionally-resilient cell state, provide avenues for future research to unravel
468 the genetic and environmental underpinnings of this complex and heterogeneous disease, with promise for
469 improving outcomes and quality of life for patients and their families.

470 **Materials and methods**

471 **Assembly of the Tissue Cohort**

472 We obtained postmortem human Brodmann Area 10 tissue from 24 schizophrenia subjects and 24 control
473 individuals matched for age, gender, and postmortem interval from the Harvard Brain Tissue Resource Center
474 at McLean Hospital. Institutional review board approval was obtained by the Harvard Brain Tissue Resource
475 Center for the collection, storage, and distribution of brain tissue and de-identified clinical information for each
476 case. Each case was assigned a consensus diagnosis by two psychiatrists based on a review of medical
477 records and a questionnaire completed by the donor's family. All cases were examined histologically, and
478 cases with neuropathology diagnosed by tissue examination were excluded. Cases were obtained through
479 family referral, and no cases were referred by a medical examiner's office. Demographic variables for the
480 assembled cohort are listed in Table S1. Upon arrival at the Harvard Brain Tissue Resource Center, fresh
481 brains were dissected, and Brodmann Area 10 tissue was identified and quickly frozen with liquid nitrogen
482 vapor prior to storage at -80°C.

483 Assessment of Medication Exposures

484 To control for the effects of psychotropic medications on disease-associated changes in gene expression,
485 medical records were reviewed and each subject's history of medication exposure was compiled for inclusion
486 in our differential gene expression analysis. Medications were clustered into categories including selective
487 serotonin reuptake inhibitors, tricyclic antidepressants, mood stabilizers, antiepileptic drugs, benzodiazepines,
488 and neuroleptics. Neuroleptic drugs were further classified by structural category, including benzisoxazoles,
489 butyrophenones, dibenzodiazepines, indoles, phenothiazines, phenylpiperazines, thienobenzodiazepines, and
490 thiothixenes. Within each medication category, the total number of distinct agents prescribed to each subject at
491 any time was input to the linear model (**Supplementary Table 1**).

492 Sample processing and single-cell RNA sequencing

493 A Nissle stained cryosection from each tissue block was examined microscopically to verify that sampled
494 tissue included all six cortical layers and underlying white matter. On dry ice 50 mg of tissue was cut from the
495 original block and stored at -80°C until further use. Tissue samples were then processed in batches of nine
496 (three schizophrenia, three control, and three samples not analyzed in the current study) using a protocol
497 adapted from a previous study²². Tissue was thawed in 0.5 ml ice-cold homogenization buffer (320 mM
498 sucrose, 5 mM CaCl₂, 3 mM Mg(CH₃COO)₂, 10 mM Tris HCl pH 7.8, 0.1 mM EDTA pH 8.0, 0.1% IGEPAL
499 CA-630, 1 mM β-mercaptoethanol, and 0.4 U μl⁻¹ recombinant RNase inhibitor (Clontech)) prior to
500 homogenization with 12 strokes in a 2 ml Wheaton Dounce tissue grinder. Tissue homogenates were passed
501 through a 40 μm cell strainer, mixed with an equal volume of working solution (50% OptiPrep density gradient
502 medium (Sigma-Aldrich), 5 mM CaCl₂, 3 mM Mg(CH₃COO)₂, 10 mM Tris HCl pH 7.8, 0.1 mM EDTA pH 8.0,
503 and 1 mM β-mercaptoethanol), layered on top of an Optiprep density gradient (750 μl 30% Optiprep solution
504 (30% OptiPrep density gradient medium, 134 mM sucrose, 5 mM CaCl₂, 3 mM Mg(CH₃COO)₂, 10 mM Tris
505 HCl pH 7.8, 0.1 mM EDTA pH 8.0, 1 mM β-mercaptoethanol, 0.04% IGEPAL CA-630, and 0.17 U μl⁻¹
506 recombinant RNase inhibitor) on top of 300 μl 40% optiprep solution (35% OptiPrep density gradient medium,
507 96 mM sucrose, 5 mM CaCl₂, 3 mM Mg(CH₃COO)₂, 10 mM Tris HCl pH 7.8, 0.1 mM EDTA pH 8.0, 1 mM β-
508 mercaptoethanol, 0.03% IGEPAL CA-630, and 0.12 U μl⁻¹ recombinant RNase inhibitor)) and centrifuged at
509 10,000 g for 10 minutes at 4°C. Nuclei were recovered from the gradient, and resuspended in an equal volume
510 of 1% BSA in phosphate buffered saline (PBS) prior to labeling with sample-specific cholesterol conjugated
511 oligonucleotide hashtags (Integrated DNA Technologies). Labeled nuclei were washed with 1% BSA in PBS
512 and pelleted by centrifugation at 500 g at 4°C for 5 minutes for three washes. After the final wash, nuclei were
513 counted on a hemocytometer, and equal numbers from each sample were combined. The pooled nuclei were
514 then applied to all eight channels of one 10x Genomics Chip B, targeting recovery of 20,000 nuclei per
515 channel. 10x Genomics and hashtag libraries were prepared as per standard 10x Genomics Chromium Single
516 Cell 3' Reagent Kits v.3 and MULTI-Seq²⁷ protocols.

517 Libraries were sequenced in batches of two on an Illumina NextSeq500 instrument (two snRNA-Seq libraries

518 and two hashtag libraries per flowcell - average 3.6E7 reads per hashtag library), and an additional round of
519 sequencing was performed for all snRNA-Seq libraries on an Illumina NovaSeq instrument (eight or 16 libraries
520 per NovaSeq S2 flowcell) to achieve an average sequencing depth of 35,142 reads per cell. Gene count
521 matrices were generated by aligning reads (including intronic reads) to the hg38 genome using 10x Genomics
522 Cell Ranger software v3.0.1 (**Supplementary Table 2**).

523 Cross-individual doublet-detection using sample hashtags

524 The deMULTiplex R package²⁷ was used to process hashtag FASTQ files, extracting 10x barcode, sample
525 hashtag, and UMI information for each read. Duplicated UMI and mismatched hashtag reads were excluded
526 and retained reads were converted to a 10x barcode by sample hashtag count matrix. This count matrix was
527 processed with the Seurat R package⁷⁶ using the HTODemux function to cluster cells based on sample
528 hashtag counts and determine a count threshold for each hashtag based on a negative binomial distribution
529 applied to the cluster with the lowest expression for that hashtag. This threshold identified each cell as positive
530 or negative for each sample hashtag, and cells identified as positive for more than one hashtag were assigned
531 as inter-sample doublets and removed from the study (**Supplementary Table 2**).

532 Characterization, visualization, and annotation of cell subpopulations using ACTIONet

533 Filtered data after doublet-detection was used as input to the archetypal analysis for cell-type identification
534 (ACTION) algorithm⁷⁷ to identify a set of transcriptional archetypes, each representing a potential underlying
535 cell type/state. Using ACTION-decompositions with varying numbers of archetypes, we employed our recently
536 developed ACTION-based network (ACTIONet) framework²⁸ to create a multi-resolution nearest neighbor
537 graph. A modified version of the stochastic gradient descent-based layout method was used in the uniform
538 manifold approximation and projection (UMAP) algorithm (Becht et al., 2018), to visualize the ACTIONet graph.
539 ACTIONet framework identifies dominant transcriptional patterns (or archetypes) and associates cells to these
540 archetypes with different degrees of confidence. To discretize cell associations, we assigned each cell to its
541 most closely associated archetype. We then used a curated set of reproducible cell-type-specific markers in
542 the human prefrontal cortex²⁸ to annotate cells assigned to each archetype.

543 To filter cells, we performed two independent iterations of the ACTIONet framework, the first one to identify
544 additional low-quality cells and missed doublets, and the second one to identify and annotate cell types/states.
545 In the first stage, we removed two archetypes that were assigned to multiple unrelated marker sets, as well as
546 cells that are not well-connected to other cells in the ACTIONet. To identify the overall connectivity of each cell
547 within the ACTIONet graph that is assigned to a given archetype, we computed its “coreness”⁷⁸ within the
548 subgraph induced by the cells associated with the same archetype. In the second round, we annotated and
549 grouped archetypes into major cell types in the human prefrontal cortex, including subtypes of excitatory and
550 inhibitory neurons, as well as non-neuronal cell types, as well as two novel schizophrenia-associated cell
551 states (**Fig. 1b,d**). We used the coreness of cells in the ACTIONet as their transparency to de-emphasize low-
552 quality cells. To verify our annotations, we projected individual marker genes for different subtypes on the

ACTIONet (**Fig. 1c**). We did not observe any batch effect and cells from all batches and both phenotypes were well-mixed in the ACTIONet plot (**Extended Data Fig. 1b, c**), and none of the archetypes is influenced by a minority of individuals, and the majority of individuals contribute to all archetypes (**Fig. 1f**).

Differential gene expression analysis using a modified pseudo-bulk approach

Following recent studies showing the success of pseudo-bulk methods for multi-sample multi-group differential analysis of single-cell datasets with complex experimental designs⁷⁹, we developed a new method based on the analysis of pseudo-bulk profiles to identify perturbed genes in schizophrenia. We aggregated the expression of genes within each archetype/individual combination and used the linear-modeling approach in the Limma package⁸⁰ to include our experimental design in the differential analysis. However, unlike the case of bulk analysis, in which the underlying variance of each gene in each sample is unknown, in single-cell pseudo-bulk analysis we can compute both the mean and the variance of genes directly from single-cells, which provides a more accurate approach than either Limma-trend or Limma-voom⁸¹. We used the inverse of the gene variances as weights in our linear model and used an outlier detection approach to mask out genes that were deemed not reliable, on a per-sample basis. For each pseudo-bulk profile, we required that it has to contain at least 50 cells to be included in our model. Finally, to account for individual-specific differences, we incorporated age, gender, PMI, batch, and medication history as covariates in our model. We filtered results based on a raw p-value cut-off of 0.05 and LFR of 0.1 to declare differential genes.

Computing transcriptional pathology scores

To assess the degree to which different cell types/states in each individual are affected by schizophrenia-associated transcriptional perturbations, we used our pseudo-bulk profiles. For each archetype, we computed a representative expression vector by averaging all pseudo-bulk samples. As a measure of schizophrenia-associated transcriptional effect in each individual/cell type, we used partial Pearson correlation between individual pseudo-bulk profiles with differential perturbation scores, after controlling for the baseline cell type/state-specific representative vector. We then scored and ranked each individual scored according to their average correlation across all archetypes.

Identification of transcriptional regulators using ChEA3

We used ChIP-X Enrichment Analysis 3 (ChEA3)⁶⁵ to prioritize transcription factors (TFs) that are likely to mediate the observed transcriptional dysregulation in schizophrenia. In summary, ChEA3 integrates multiple libraries of putative TF-target lists, gathered from different sources, including TF-gene co-expression from RNA-seq studies, TF-target associations from ChIP-seq experiments, and TF-gene co-occurrence computed from crowd-submitted gene lists, to compute a composite ranked list of TFs. We used the *TopRank* strategy to combine rankings from individual libraries, in which the best scaled-rank of each TF across all libraries is used to aggregate TF scores. We report the log-transformed scaled-rank as the relevance measure of each TF by ChEA3 analysis.

587 Gene-centric analysis of common variants using H-MAGMA

588 Hi-C-coupled MAGMA (H-MAGMA) is a recent extension of the traditional multimarker analysis of genomic
589 annotation (MAGMA), a method developed to prioritize genes by aggregating single nucleotide polymorphism
590 associations to nearest genes. In H-MAGMA, the linking of SNPs to genes is extended to include long-range
591 interactions brought together through the chromatin looping. In our analysis, we used the preprocessed dataset
592 of SNPs-gene links based on the Hi-C data in the adult human brain.

593 Fluorescence *in situ* hybridization (FISH)

594 From our larger cohort of postmortem human BA10 tissue, six cases were selected for FISH experiments
595 including CON10, CON14, SZ5, SZ12, SZ20, and SZ23. Frozen tissue blocks were embedded in optimal
596 cutting temperature medium (OCT), and 10 µm sections were cut at -20 °C with a Microm HM560 cryostat,
597 mounted on Superfrost Plus slides (one control, one schizophrenia, and one transcriptionally-resilient case
598 mounted on each slide to ensure balanced processing) and stored -80°C until FISH was conducted.

599 Advanced Cell Diagnostics (ACD) designed the *in situ* hybridization probes (human *SHANK2*, *UNC13A*, *TCF4*,
600 and *CLU*) as well as the positive and negative control probes (**Supplementary Table 14**). The RNAscope
601 Multiplex Fluorescent Reagent Kit v2 (ACD) was used for the assay following the manufacturer's instructions
602 with some modifications. Nuclei were counterstained with DAPI using TSA buffer (ACD) and TSA Plus
603 fluorophores (PerkinElmer). Briefly, frozen sections were fixed for 1 h at 4 °C using freshly prepared ice-cold
604 10% neutral buffered formalin, and rinsed with phosphate buffered saline (PBS) and dehydrated in 50%, 70%,
605 and two changes of 100% ethanol (5 min each) at room temperature (RT). Sections were air-dried and a
606 hydrophobic barrier drawn around each section with an Immedge pen (Vector Laboratories). When completely
607 dry, sections were treated with hydrogen peroxide for 10 min at RT, washed twice with PBS, incubated with
608 protease IV for 15 min at RT, and washed again twice with PBS.

609 After diluting the probes for RNA detection 1:50, sections were hybridized with the probes (40°C, 2 h; HybEZ
610 Hybridization System (ACD)), washed twice, and stored overnight at RT in 5x SSC buffer. The following day,
611 slides were washed twice with the wash buffer, followed by three amplification steps (AMP 1 (30 min), AMP 2
612 (30 min), and AMP 3 (15 min); 40°C). Each amplification step was followed by two washes of 2 min each with
613 the wash buffer. Sections were then incubated sequentially with the HRP reagent corresponding to each
614 channel (e.g. HRP-C1; 40°C, 15 min) followed by the respective TSA Plus fluorophore assigned to the probe
615 channel (Opal dyes, 520, 620 and 690, dilution 1:1500; 40°C, 30 min) and HRP blocker (40°C, 15 min), and
616 each incubation was followed by two wash steps. Lipofuscin autofluorescence was visible in both green and
617 red channels. Since the far-red channel showed less autofluorescence, highly expressed *UNC13A-C4* and
618 *CLU-C2* probes were assigned to the green fluorescein channel and the *CUX2* layer-specific marker was
619 assigned to the red cyanine 5 channel. DAPI (30 s) was used to visualize cell nuclei. Sections were mounted
620 using ProLong Gold mounting medium (Thermo Fisher Scientific) and stored at 4 °C. Two independent
621 experiments were performed, with three biological replicates each, and positive and negative control probes to

622 test for RNA quality and background signal, respectively.

623 Leica Laser Scanning Confocal Microscopy

624 Image acquisition, processing, and quantitation were performed blind to diagnosis. All microscopy was
625 performed at the Microscopy Core at McLean Hospital on a Leica TCS-SP8 confocal microscope. Exposure
626 times were set separately for each of the four channels (red for Cy5, blue for DAPI, green for FITC, and orange
627 for Texas Red) and kept similar among the cases to enable comparison. Images at 40x and 63x magnifications
628 were visualized as maximum intensity projections of Z-stacks at 1.5 μm intervals. Two representative fields of
629 view were selected within cortical layers II and III as identified by positive *CUX2* staining, and Z-stacks were
630 taken throughout the depth of single cells, with ≥ 40 single cells per case and six cases per target gene.
631 Adjustment of brightness, contrast, and sharpness was done using Adobe Photoshop. Quantification of
632 transcripts was performed in an automated unbiased manner using dotdotdot⁴⁰. For all six cases, the dotdotdot
633 MATLAB script (<https://github.com/LieberInstitute/dotdotdot>) was used to process one 40x and one 63x
634 maximum intensity projection image, counting the number of puncta in each channel overlapping with each
635 region of interest (nucleus) identified by DAPI staining. Data presented in figure 2e represent counts of *TCF4*,
636 *CLU*, *SHANK2*, and *UNC13A* transcripts within individual nuclei containing at least one detected *CUX2*
637 transcript, and excluding counts of zero.

638 CUT&Tag mapping of transcription factor binding in the neuronal genome

639 Nuclei were isolated from the postmortem human prefrontal cortex as described above and incubated with
640 1:1000 diluted anti-NeuN antibody (EMD Millipore MAB377X) with 0.5% BSA in PBS at 4°C with end-over-end
641 rotation for 45 minutes. After staining nuclei were counterstained with propidium iodide and sorted on a BD
642 FACSria III Cell Sorter at Harvard University's Bauer Core Facility. 100,000 neuronal nuclei were used as
643 input for each Cleavage Under Targets and Tagmentation (CUT&Tag) assay using rabbit primary antibodies
644 targeting MEF2C (Abcam ab211439), SATB2 (Abcam ab92446), SOX5 (Abcam ab94396), TCF4 (ProteinTech
645 22337-1-AP), H3K27Ac (EMD Millipore MABE647), and mouse-anti-rabbit secondary antibody (Sigma R2655)
646 with the Vazyme pG-Tn5 CUT&Tag kit (Cellagen Technology, San Diego) according to the manufacturer's
647 protocol. CUT&Tag libraries were sequenced on one NextSeq500 flow cell at the MIT BioMicroCenter. Reads
648 were aligned to the HG38 genome, processed to bedgraph format, and analyzed with the Sparse Enrichment
649 for CUT&Run⁸² tool with "stringent" parameters retaining the top 1% of peaks.

650 Acknowledgements:

651 We thank the individuals and families whose donation of human brain tissue made this work possible. This
652 work was supported by the Wilf Family Foundations and by NIH grant K08MH109759 (W.B.R.) and by NIH
653 grants 1U01MH119509, R01MH109978, and R01AG062335 (M.K.).

654 Author Contributions:

655 This study was designed by W.B.R., and directed and coordinated by W.B.R. and M.K. W.B.R., S.S., and

656 D.R.T. performed the snRNA-seq experiment, S.S. performed the RNAScope experiment and W.B.R. and S.S.
657 performed the CUT&Tag experiment. W.B.R. performed data processing and S.M. and J.D.-V. performed the
658 computational analysis. D.R.T. and M.H. reviewed medical records under supervision of W.B.R. W.B.R., S.M.,
659 J.D.-V., and M.K. wrote the manuscript.

660 **Data Availability:**

661 The MULTI-seq data are available at Synapse (<https://www.synapse.org/#!/Synapse:syn22963646>). The data
662 are available under controlled use conditions set by human data privacy regulations, and access requires a
663 data use agreement to ensure the anonymity of the donors of postmortem human brain tissue. A data use
664 agreement can be pursued with SAGE, who maintains Synapse and can be downloaded from their website.

665 **Supplementary Tables**

- 666 1. Subject demographics and medications (TableS1_SubjectDemographics&Medication.xlsx)
- 667 2. Sequencing statistics (TableS2_SequencingMetrics.xlsx)
- 668 3. Cell-type/state-specific marker genes (TableS3_Combined_marker_tables.xlsx)
- 669 4. Marker gene comparison between Ex-L5/6-CCa and Ex-L5/6-CCb (TableS4_CCb_scores.xlsx)
- 670 5. Pathways enriched in top-ranked marker genes from each cell-type/state
671 (TableS5_Combined_marker_tables_enrichments.xlsx)
- 672 6. Up- (TableS6a_up_regulated_genes.xlsx) and down- (TableS6b_down_regulated_genes.xlsx)
673 regulated genes in schizophrenia
- 674 7. Pseudo-bulk mean (TableS7a_Pseudobulk_mean.xlsx) and variance
675 (TableS7b_Pseudobulk_variance.xlsx) profile per cell type/state, and computed Transcriptional
676 Pathology Scores for each subject (TableS7c_TPS_scores.xlsx)
- 677 8. Curated set of neuro-associated functional pathways (NFP) and member genes (TableS8a_NFP.xlsx),
678 and functional pathway enrichment of up- (TableS8b_DE_up_gprofiler.xlsx) and down-
679 (TableS8c_DE_down_gprofiler.xlsx) regulated genes
- 680 9. Schizophrenia GWAS loci linked to DEGs (TableS9_GWAS_SNP_table.xlsx)
- 681 10. ChEA scores for association of 1632 TFs with up- and downregulated genes
682 (TableS10_ChEA_scores.xlsx)
- 683 11. NFP enrichment of TFs associated with dysregulated genes
684 (TableS11a_ChEA_TFs_enrichment_NFP.xlsx), and functional pathway enrichment of TFs associated
685 with the set of up- (TableS11b_ChEA_TFs_up_gprofiler.xlsx) and down-
686 (TableS11c_ChEA_TFs_down_gprofiler.xlsx) regulated genes
- 687 12. Filtered and normalized profile of the merged pseudo-bulk mean profiles
688 (TableS12_FilteredNorm_JointPseudobulk.xlsx), used for TF expression correlation analysis
- 689 13. TF membership of individual regulons (TableS13_Regulons.xlsx)
- 690 14. RNAScope targets, probes, channels, and fluorophores (TableS14_RNAScopeProbes.xlsx)

Figure 1

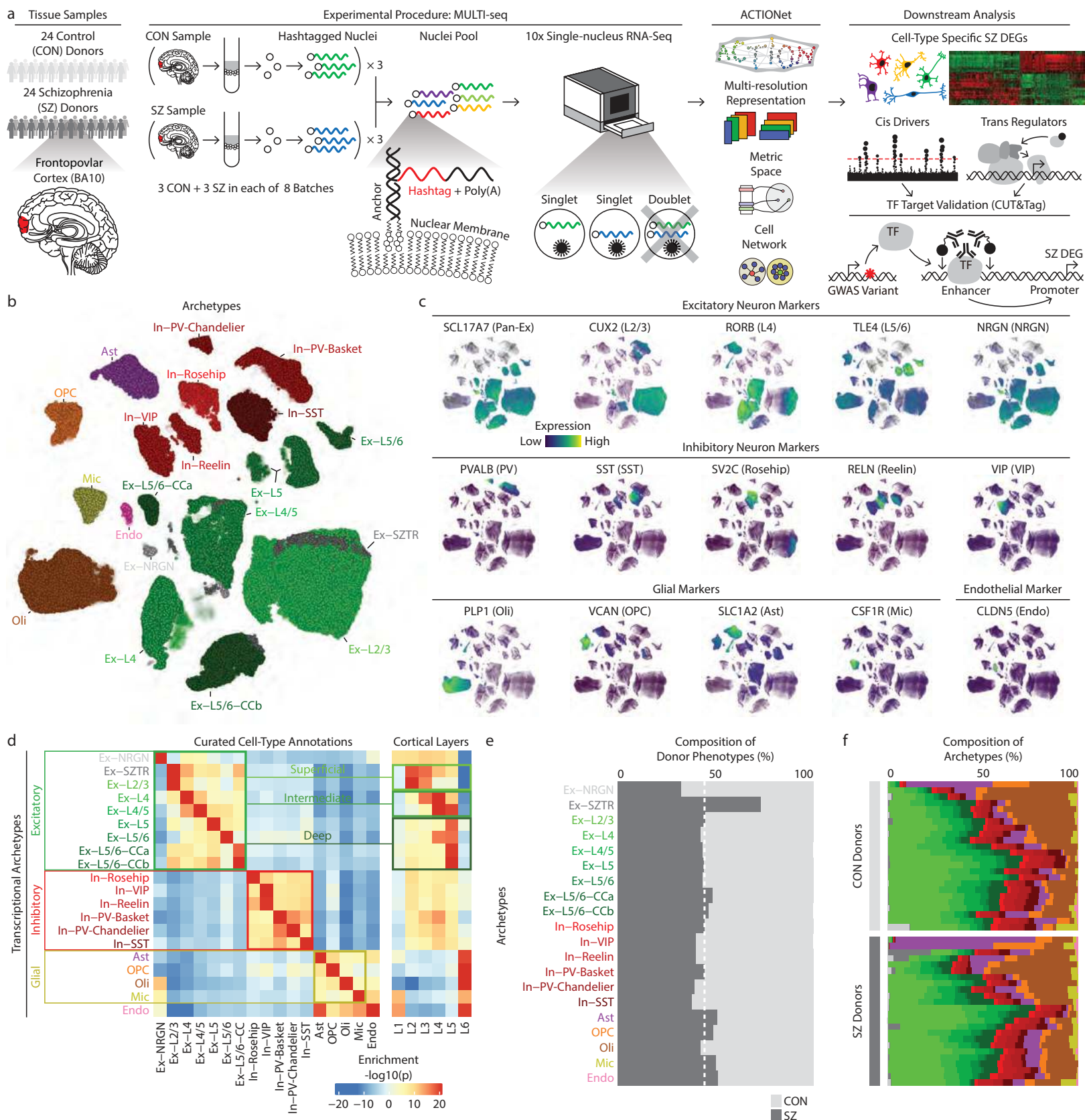


Figure 1. Multiresolution dissection of cellular subpopulations. **a.** Overview of study design and data analysis strategies. TF - transcription factor. CUT&Tag - Cleavage Under Targets and Tagmentation. **b.** ACTIONet plot of putative cell types/states. Green and red clusters represent excitatory and inhibitory subtypes of neurons respectively, with darker shades indicating an association with deeper cortical layers. **c.** Projection of known marker genes verifies cell type annotations and cortical layer associations⁸². **d.** Annotation of transcriptional archetypes using curated markers from previous studies. **e.** The percentage of cells within each cell-type/state contributed by SZ and CON subjects. **f.** Cell-type/state decomposition of individual samples. Colors are consistent with those used in panel b.

Figure 2

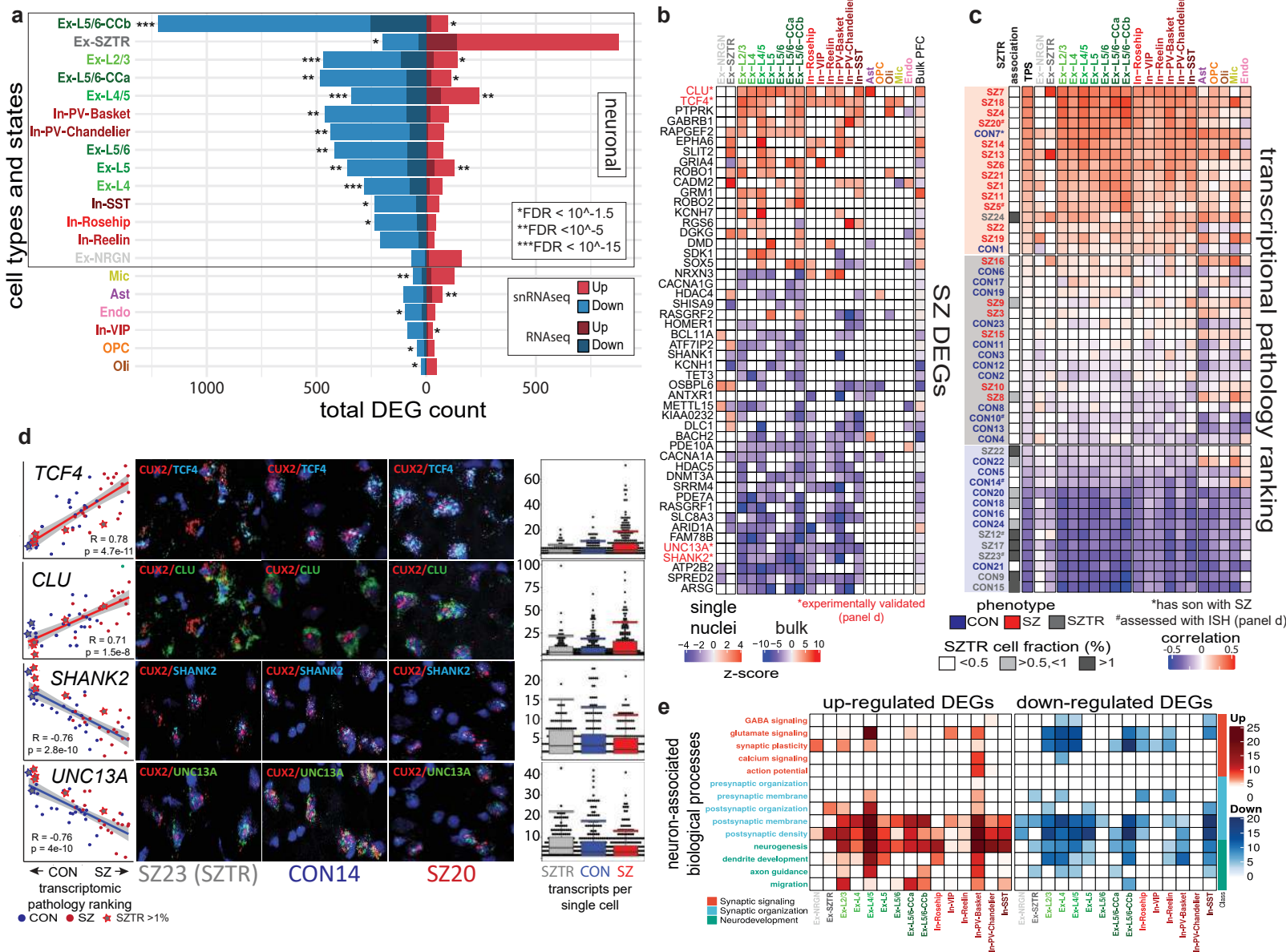


Figure 2. Differential gene expression analysis. **a.** Total count of up- and down-regulated genes in each cell-type/state and the overlap of cell-type/state-specific SZ DEGs with DEGs observed in previous studies of bulk cortical tissue²⁸. **b.** Cell-type-specific differential expression of selected top-ranked genes across all 20 cell-types/states as well as previous studies of bulk cortical tissue. Many selected genes demonstrate consistent up or downregulation across most cell populations, while others show distinct patterns across major categories (*NRXN3*, *RASGRF2*, *BACH2*, *DMD*), and several genes are dysregulated in opposite directions within Ex-SZTR and multiple neuronal cell-types (*GRIA4*, *DLC1*, *KIAA0232*, *HDAC4*, *ATF7IP2*). Blue indicates downregulation, and red indicates overexpression in SZ. Comparisons with nominal $p > 0.05$ are not colored. **c.** Ranking of individuals based on an aggregate Transcriptional Pathology Score computed across all neuronal cell-types/states. Red indicates a transcriptomic signature more typical of SZ, while blue indicates a signature more typical of CON. *Individual CON7 has a first degree relative with SZ. **d.** The first column depicts the relative pseudobulk expression across all neuronal cell-types of *TCF4*, *CLU*, *SHANK2*, or *UNC13A* on the y-axis plotted against the transcriptomic pathology score ranking of each subject on the x-axis. Columns two through four show representative photomicrographs of fluorescent in situ hybridization for *CUX2* in red, a marker of excitatory neurons in layers II and III of the cortex, and *TCF4*, *CLU*, *SHANK2*, or *UNC13A* in blue or green. Column five depicts quantitation of the in situ hybridization signal as detected transcripts per single *CUX2* positive cell using DotDotDot⁷⁶. Points indicate individual cell counts, boxes indicate the median and the interquartile range, and whiskers indicate the largest value within 1.5 times the interquartile range above the 75th percentile. **e.** Functional enrichment of cell-type/state-specific SZ DEGs within neuronally relevant biological processes.

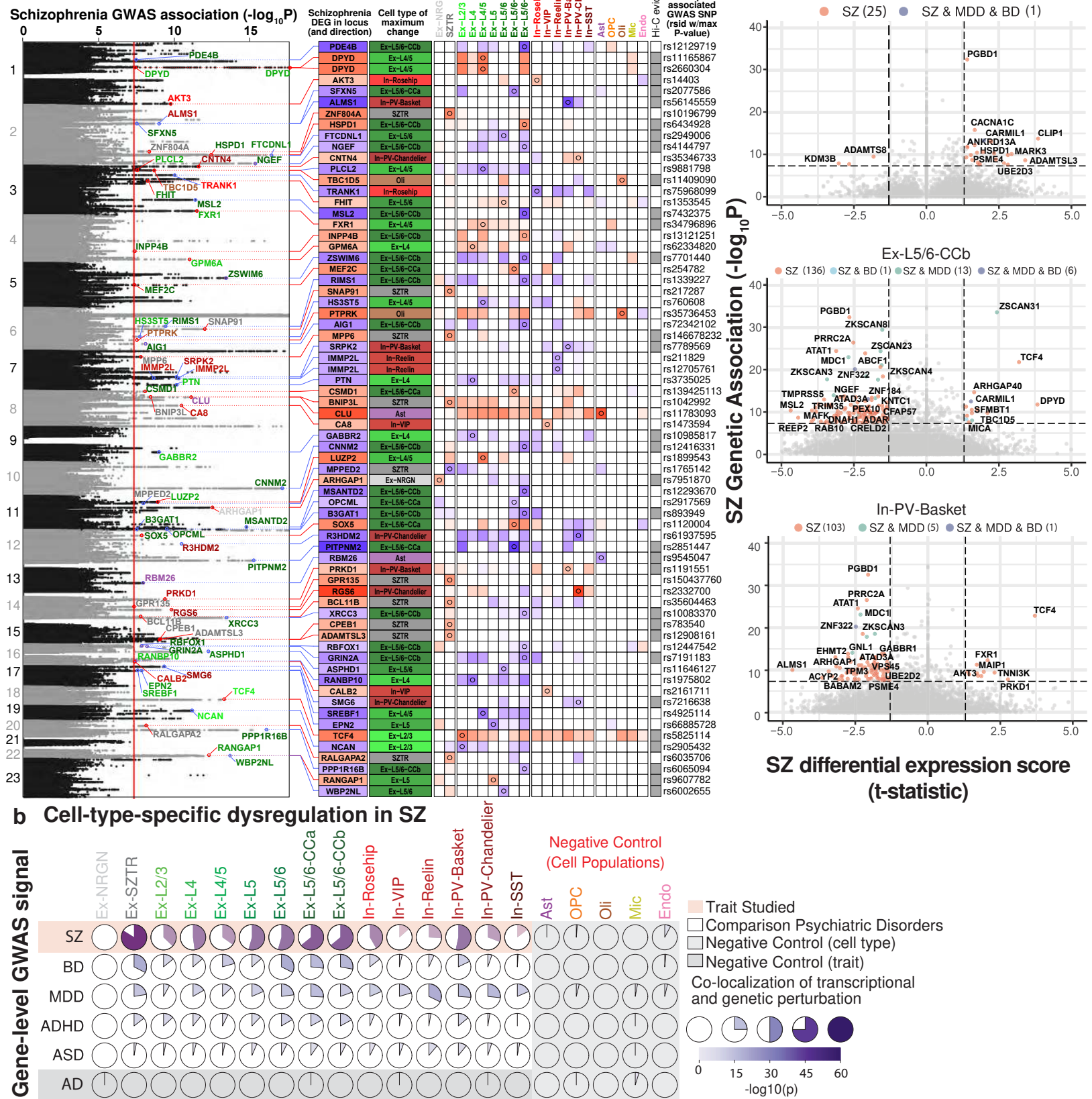


Figure 3. Correlation of differentially expressed genes with GWAS-associated genesets. a. Schizophrenia DEGs suggest mechanisms of action for 68 of 145 GWAS implicated loci. Shown are the 68 GWAS loci¹⁴ containing significant SZ DEGs, along with the most perturbed gene, the cell-type in which the largest DE event occurs, and a heatmap depicting all DE events for that gene within neuronal populations (red - upregulated; blue - downregulated, circles mark the maximum differential expression event for each gene). **b.** Correlation plots depicting the overlap between cell-type/state-specific schizophrenia DEGs and genes implicated by Genome-Wide Association Studies of six distinct neuropsychiatric disorders. Within each pairwise association, the ratio of purple clock-face indicates the relative amount of overlap, with the intensity of coloring indicating the significance of the association. **c.** Visualization of the relationship between the level of significance of genome-wide association with schizophrenia (y-axis) and the magnitude of differential expression in schizophrenia (x-axis) for individual genes within three neuronal populations.

Figure 4

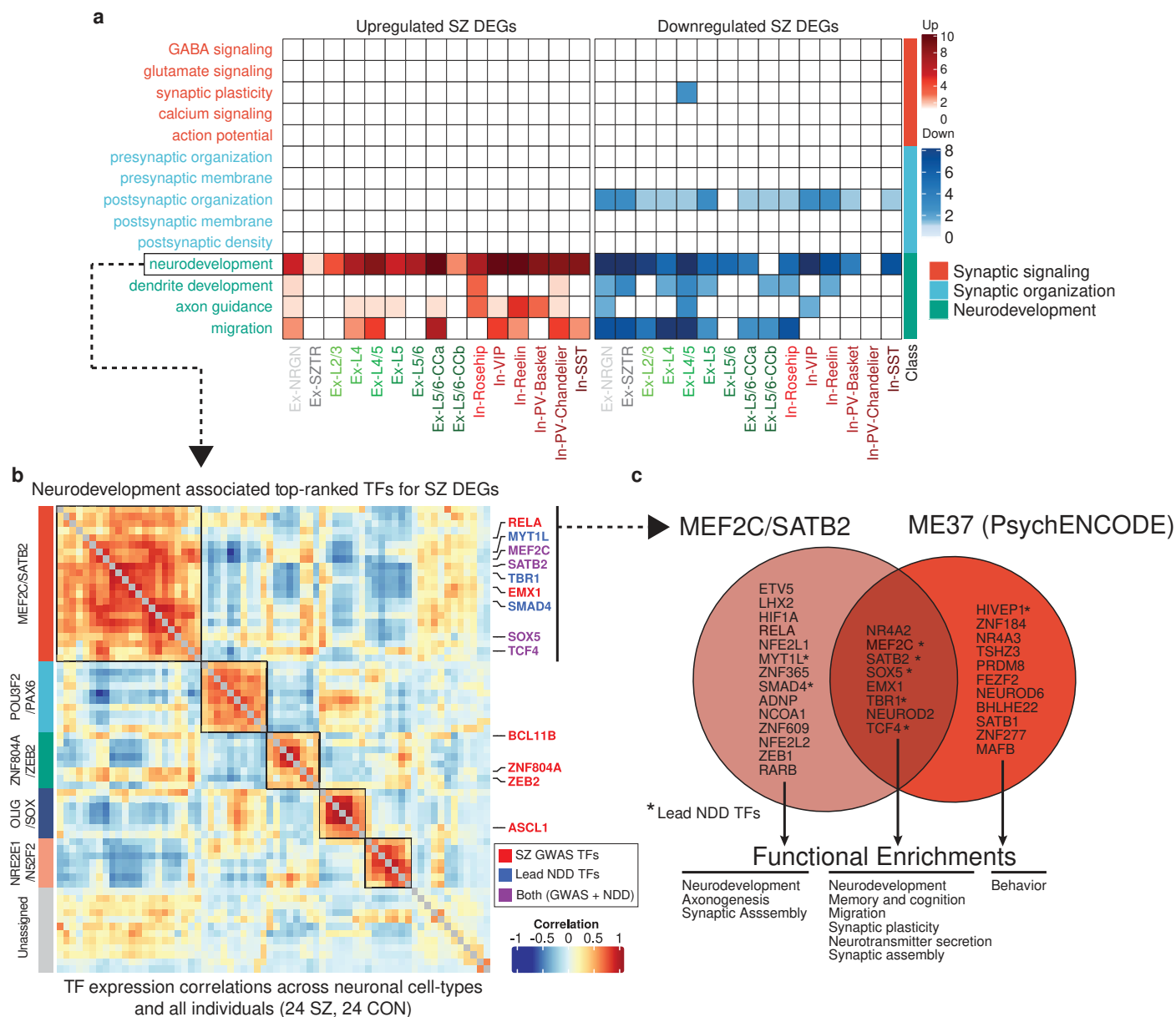
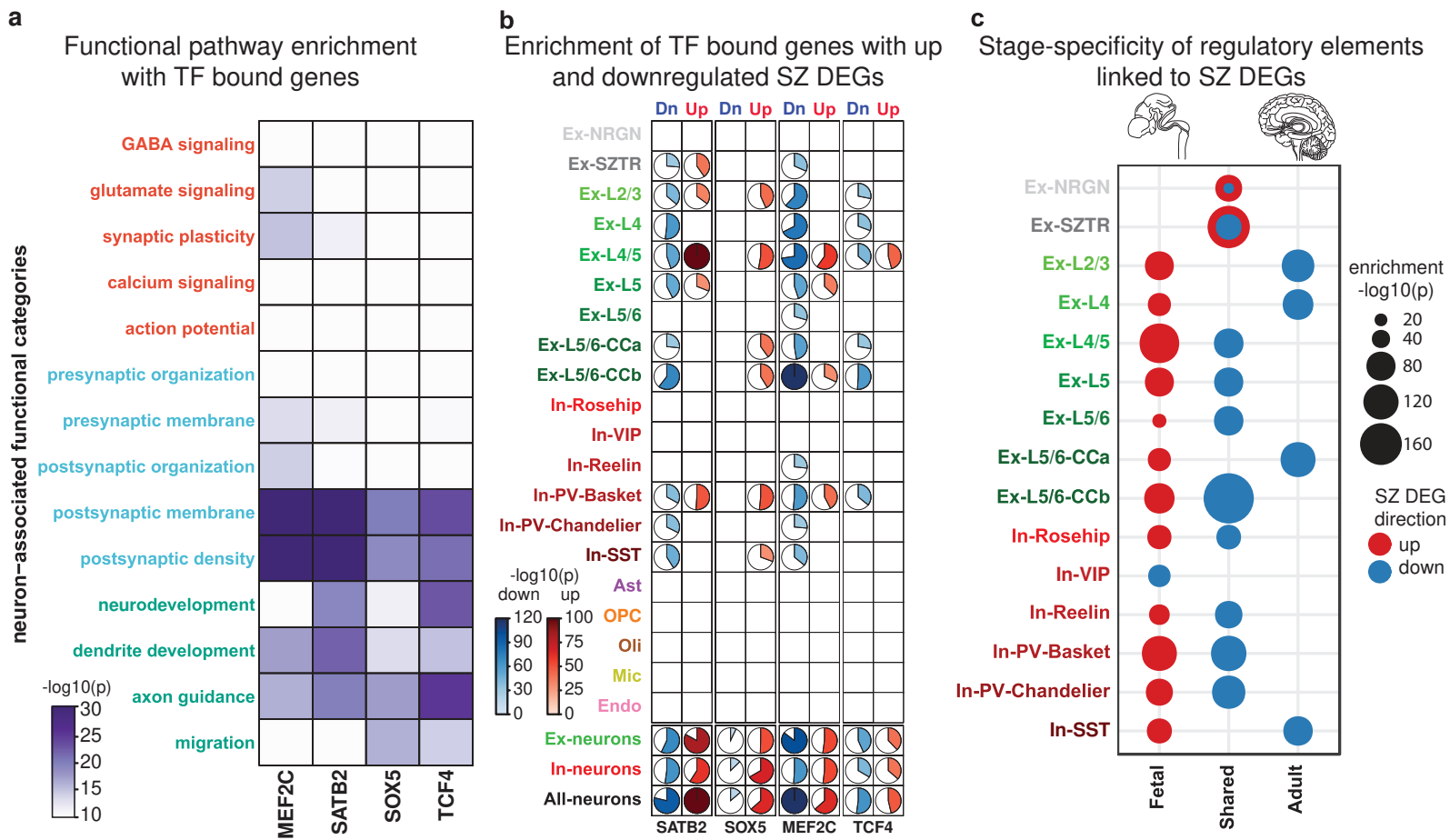
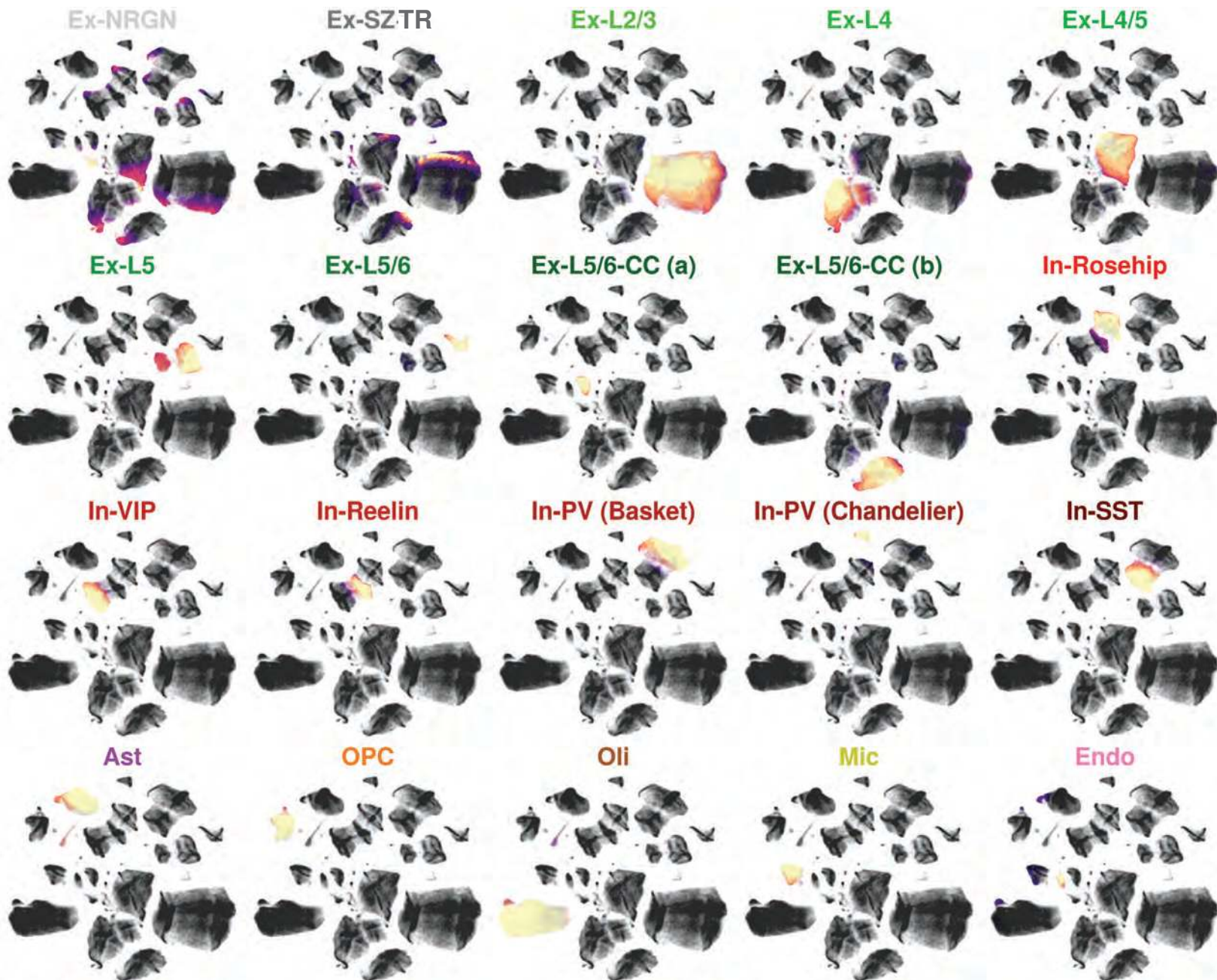


Figure 4. Schizophrenia-associated transcriptional regulators. **a.** Functional enrichment of the top-ranked transcriptional regulators identified by ChEA3 analysis. **b.** Co-expression heatmap of the most perturbed neurodevelopmentally-driven TFs across pseudobulk profiles from all cell-types/states and all individuals identifies five distinct TF modules, with high enrichment of GWAS-associated TFs in the MEF2C/SATB2 module (boxed top left). **c.** Overlap of TFs within the MEF2C/SATB2 module and the ME37 module identified in the PsychENCODE brain development dataset.

Figure 5

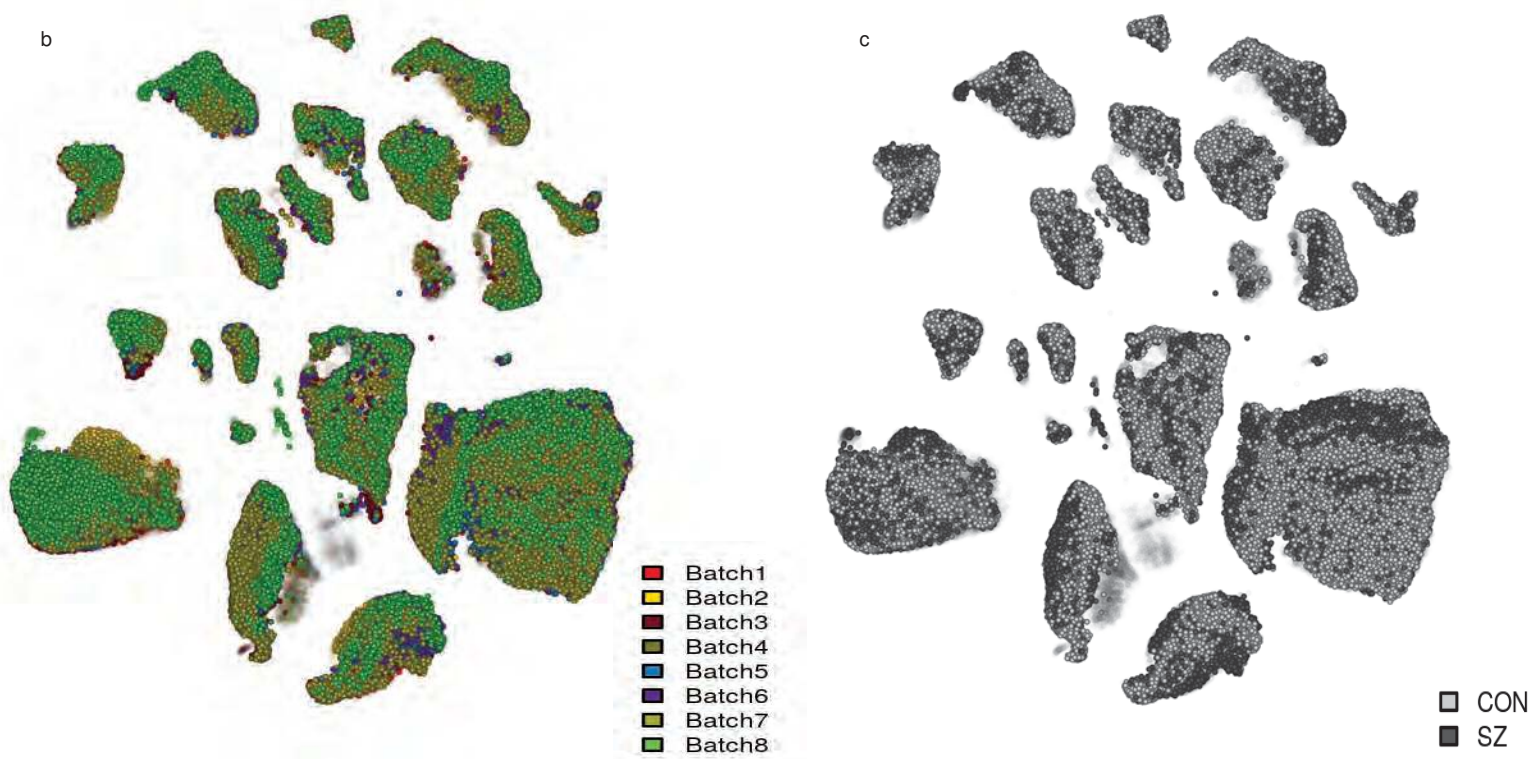


Extended Data Figure 1a. ACTIONet cell-cell similarity network depicting the footprint of all 20 identified transcriptional archetypes



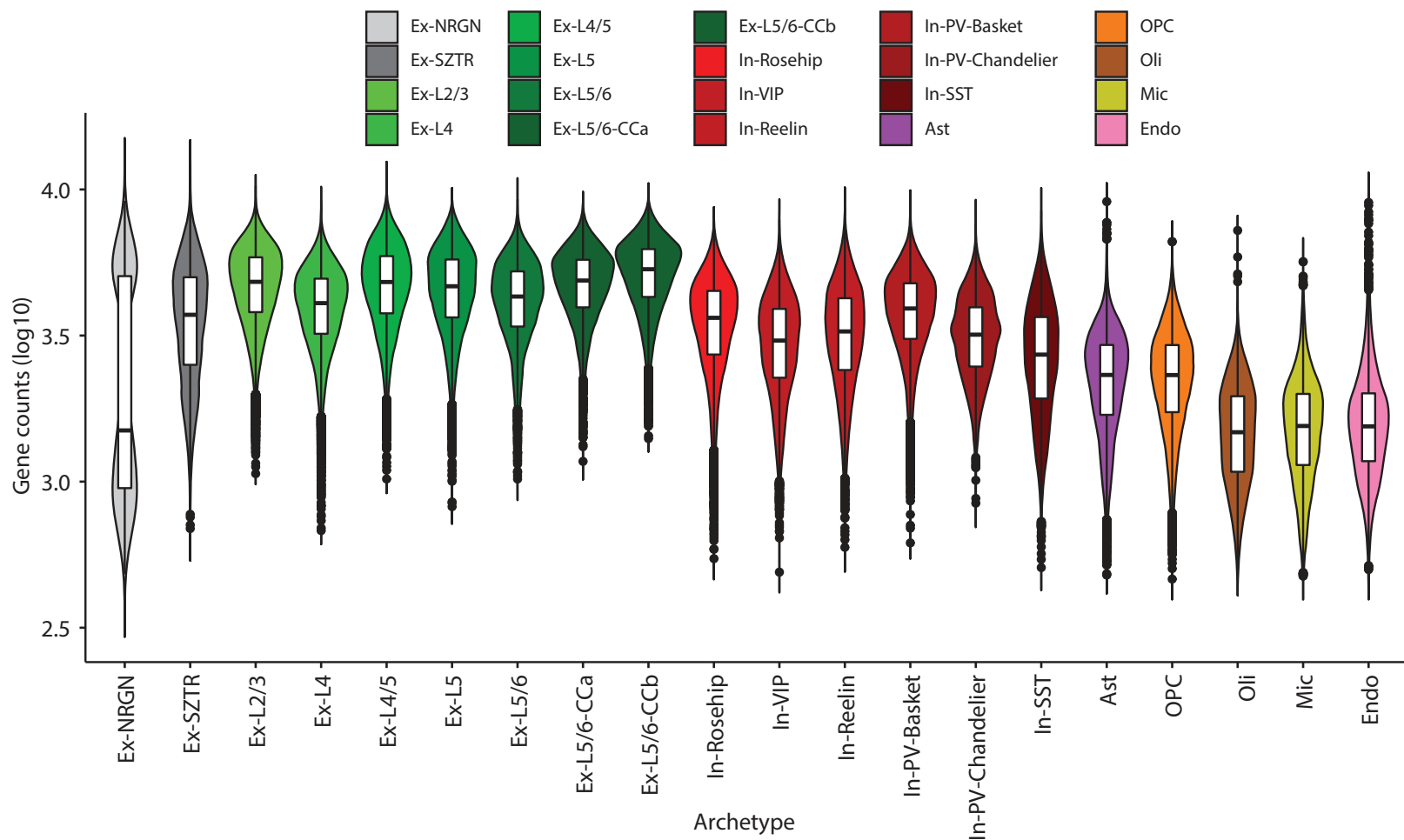
Extended Data Fig. 1 ACTIONet cell-cell similarity network. Network-based two-dimensional visualization of all cells considered in the analysis (n=560,020) indicating association with identified transcriptional archetypes.

Extended Data Figure 1b,c. ACTIONet cell-cell similarity network colored by 10x batch (left) or phenotype (right)



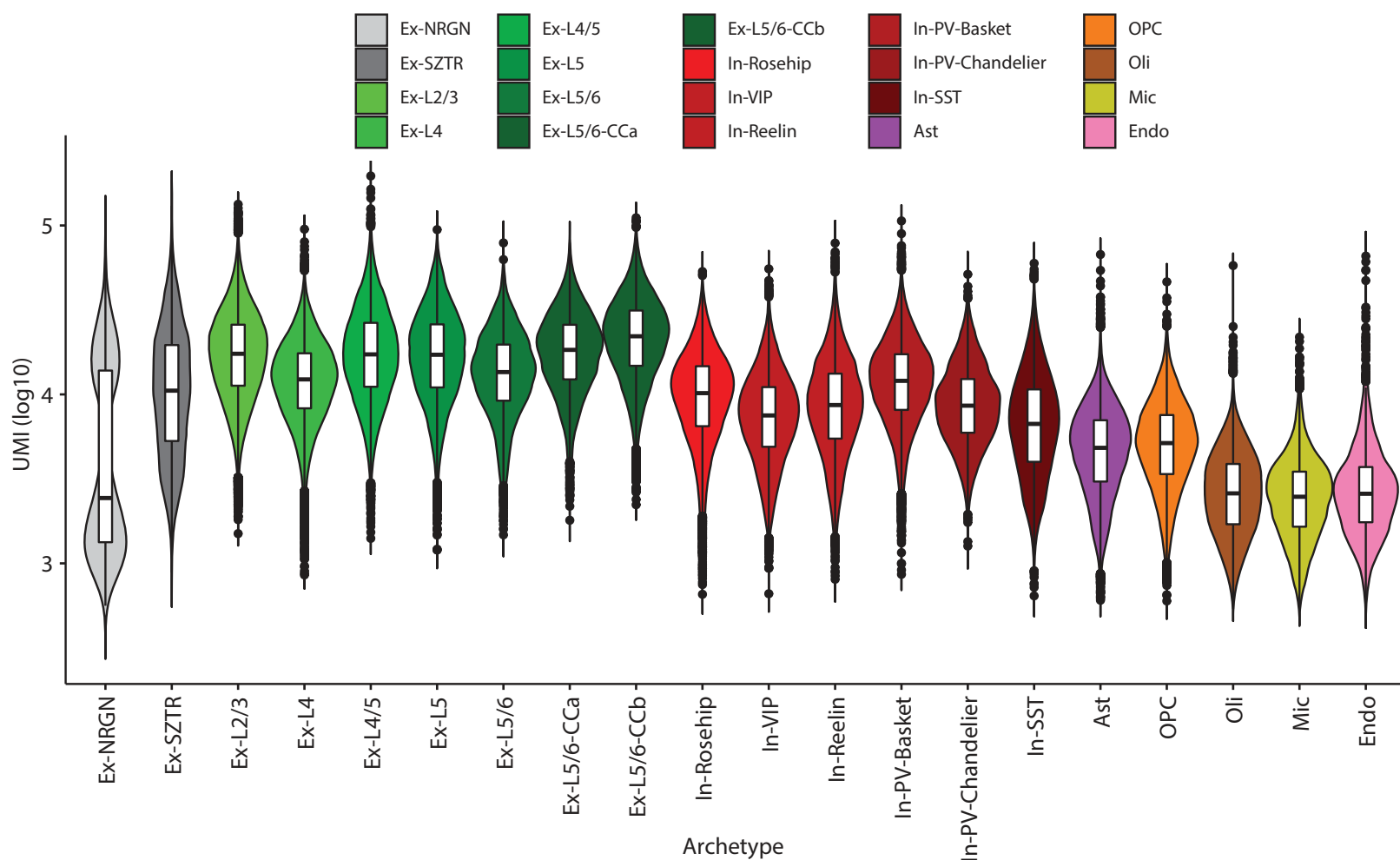
Extended Data Fig. 1b,c. ACTIONet cell-cell similarity network. Network-based two-dimensional visualization of all cells considered in the analysis ($n=560,020$) indicating association with 10x batch (b), or phenotype (c) (SZ:schizophrenia, $n=266,431$; CON: control, $n=293,589$).

Extended Data Figure 2a. Gene capture across cell-types



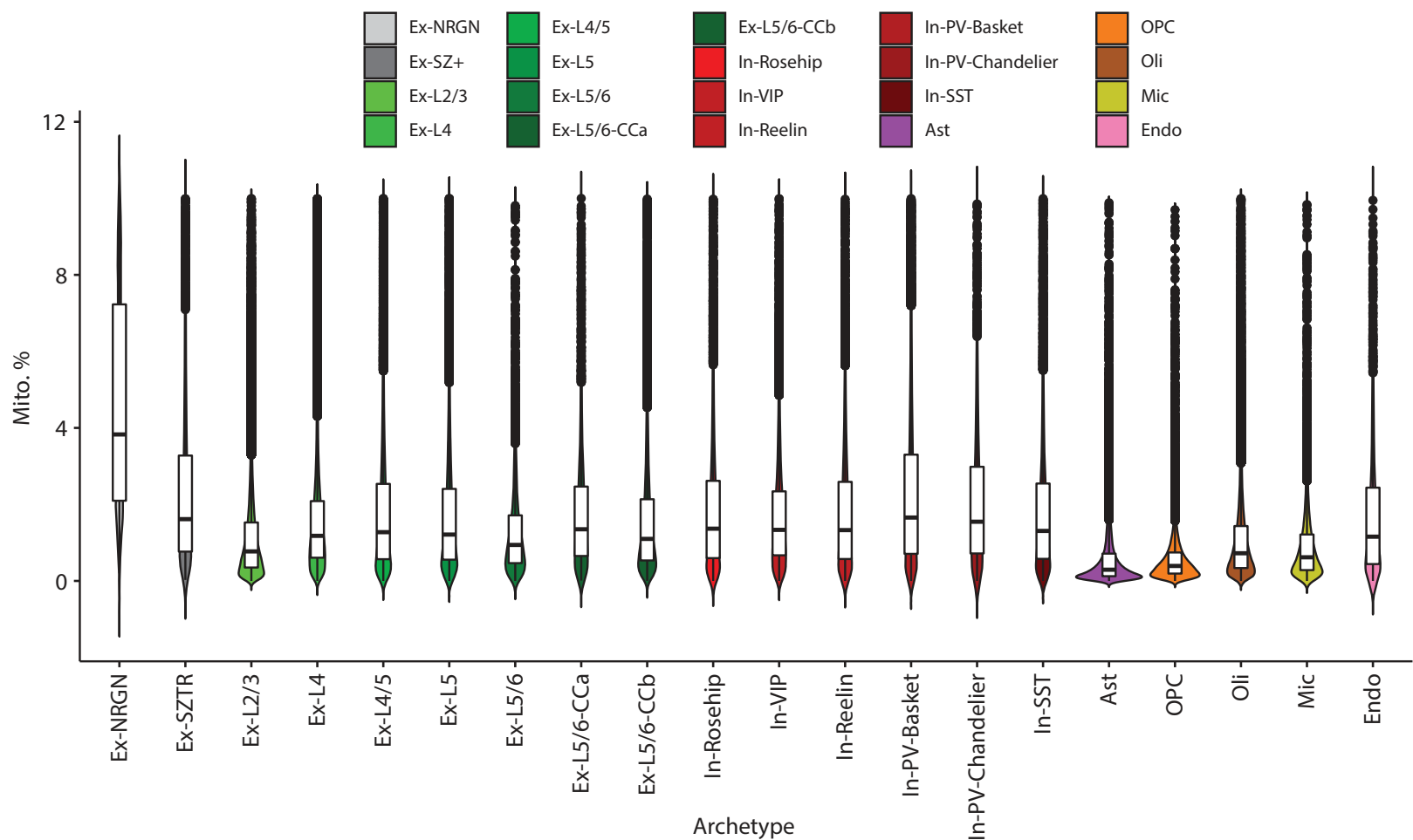
Extended Data Fig. 2a Cell type gene and cell statistics. Gene count distribution across cells of each type. Each point represents in log scale the number of genes detected to have a read count $x > 0$ in a given cell. Box plots are centred around the median, with the interquartile range (IQR) defining the box. The upper whisker extends to the largest value no further than $1.5 \times$ IQR from the end of the box. The lower whisker extends to the smallest value at most $1.5 \times$ IQR from the end of the box.

Extended Data Figure 2b. UMI capture across cell-types



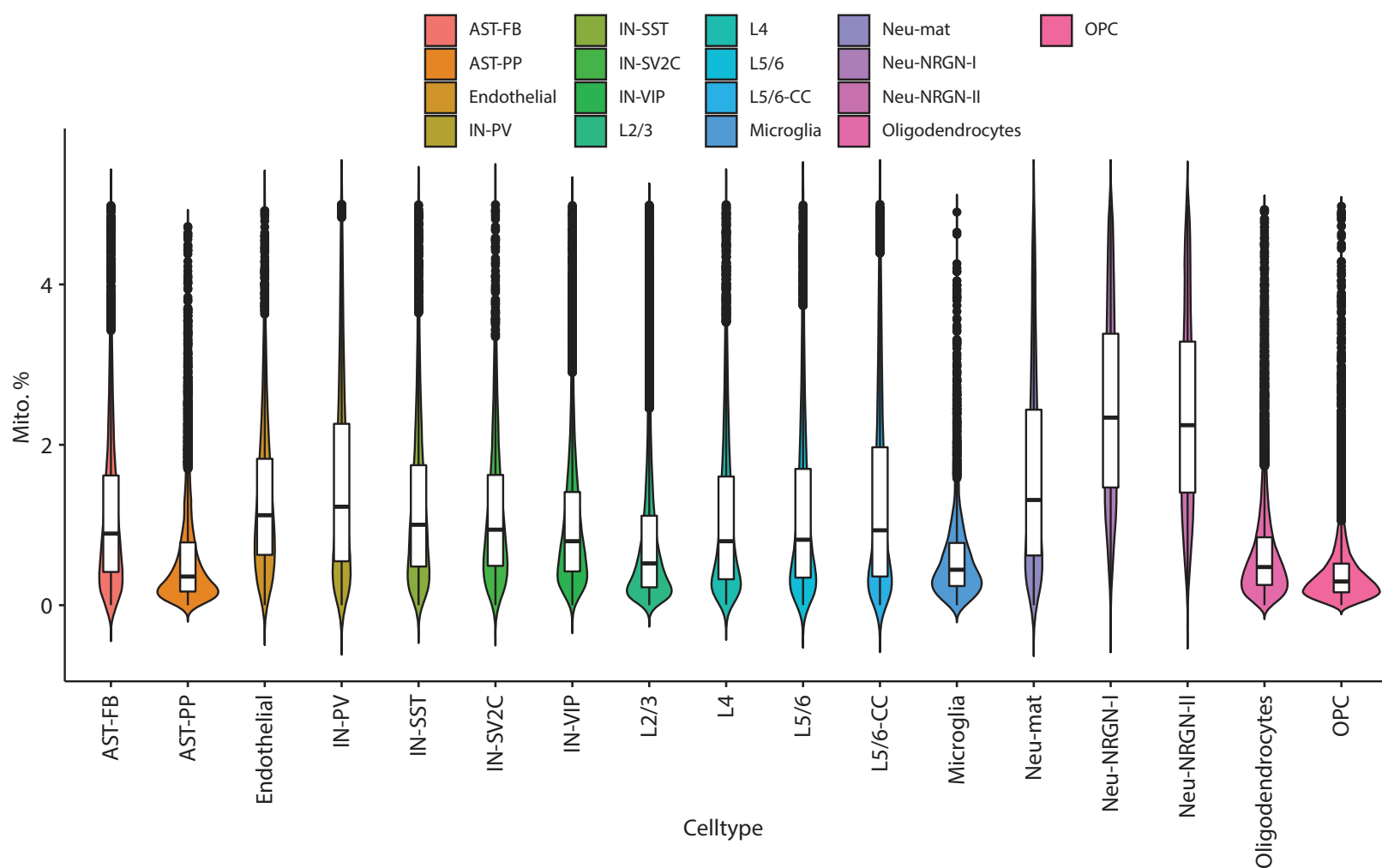
Extended Data Fig. 2b Cell type gene and cell statistics. Total UMI count distribution across cells of each type. Each point represents the total UMI count across all genes in a given cell. Box plots are centred around the median, with the interquartile range (IQR) defining the box. The upper whisker extends to the largest value no further than $1.5 \times$ IQR from the end of the box. The lower whisker extends to the smallest value at most $1.5 \times$ IQR from the end of the box.

Extended Data Figure 2c. Mitochondrial gene capture across cell-types



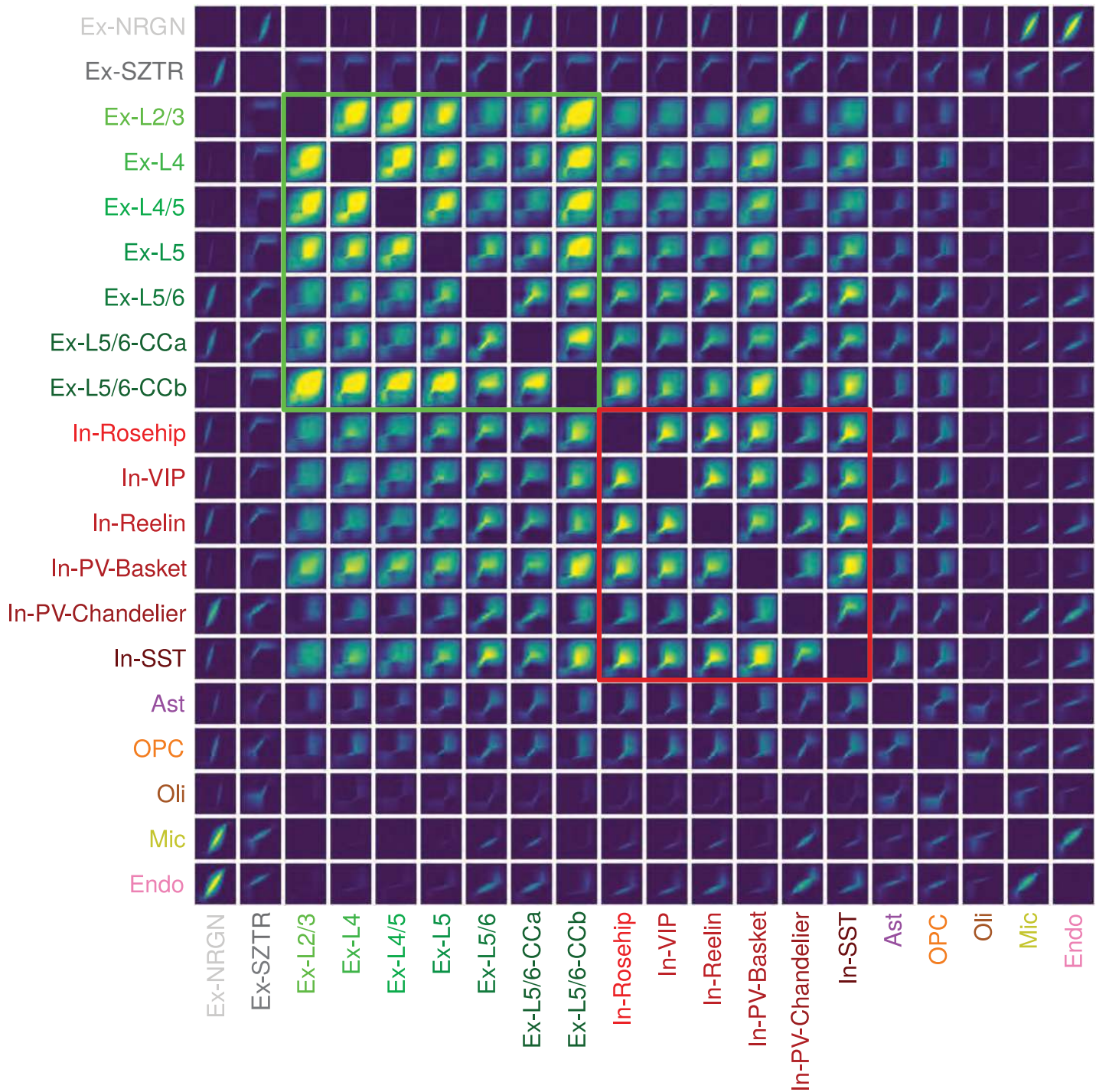
Extended Data Fig. 2c Cell type gene and cell statistics. Distribution of UMI percentages that map to mitochondrially encoded genes across cells of each type. Distributions are shown for the SCZ dataset reported herein. Box plots are centered around the median, with the interquartile range (IQR) defining the box. The upper whisker extends to the largest value no further than $1.5 \times$ IQR from the end of the box. The lower whisker extends to the smallest value at most $1.5 \times$ IQR from the end of the box.

Extended Data Figure 2d. Mitochondrial gene capture across cell-types in the Velmeshev 2019 dataset






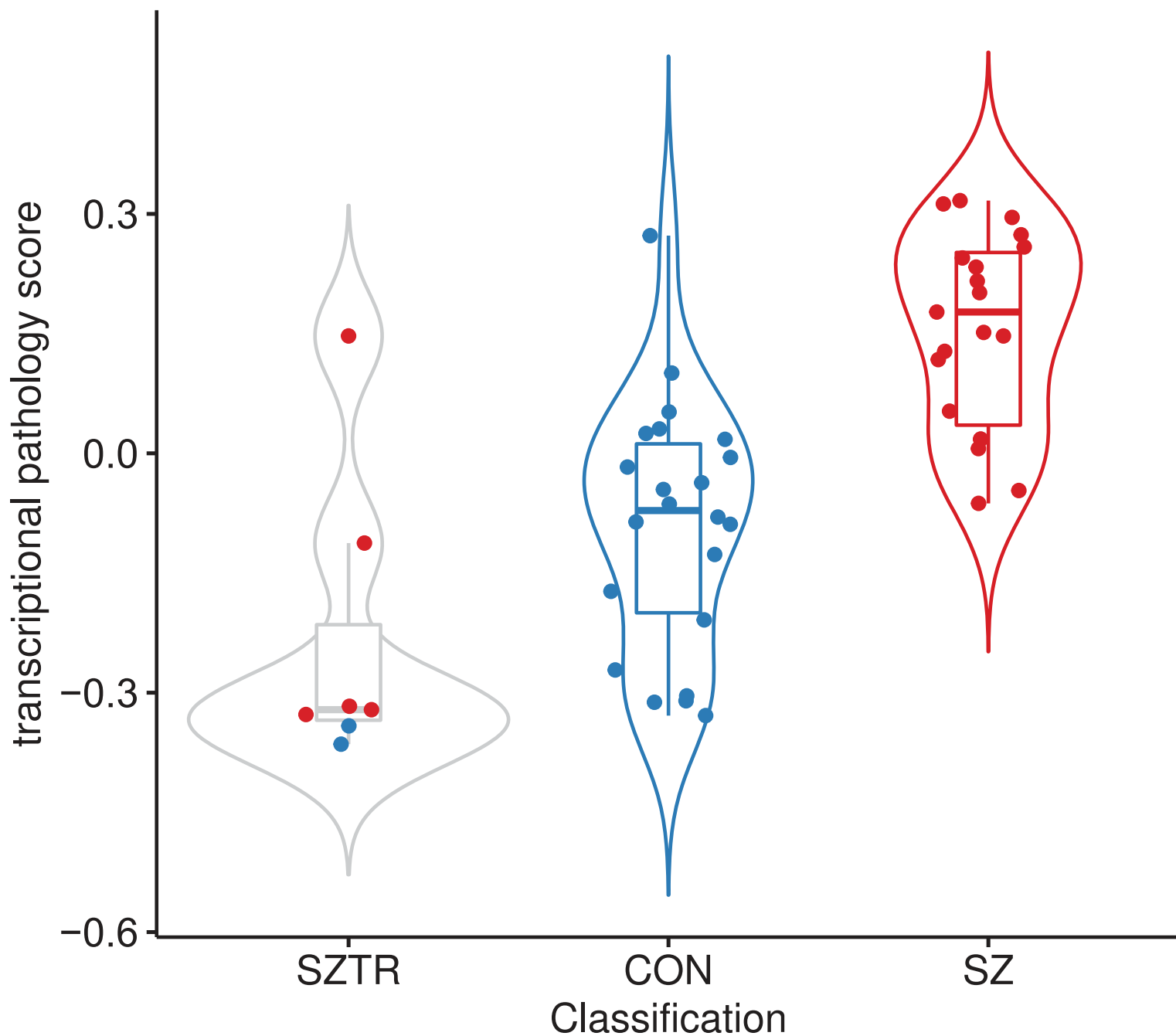
Extended Data Fig. 2d Cell type gene and cell statistics. Distribution of UMI percentages that map to mitochondrially encoded genes across cells of each type. Distributions are shown for the dataset reported in Velmeshev et al. 2019. Box plots are centred around the median, with the interquartile range (IQR) defining the box. The upper whisker extends to the largest value no further than $1.5 \times \text{IQR}$ from the end of the box. The lower whisker extends to the smallest value at most $1.5 \times \text{IQR}$ from the end of the box.

Extended Data Figure 3. Rank-Rank Hypergeometric Overlap Plot of cell-type-specific transcriptomic changes



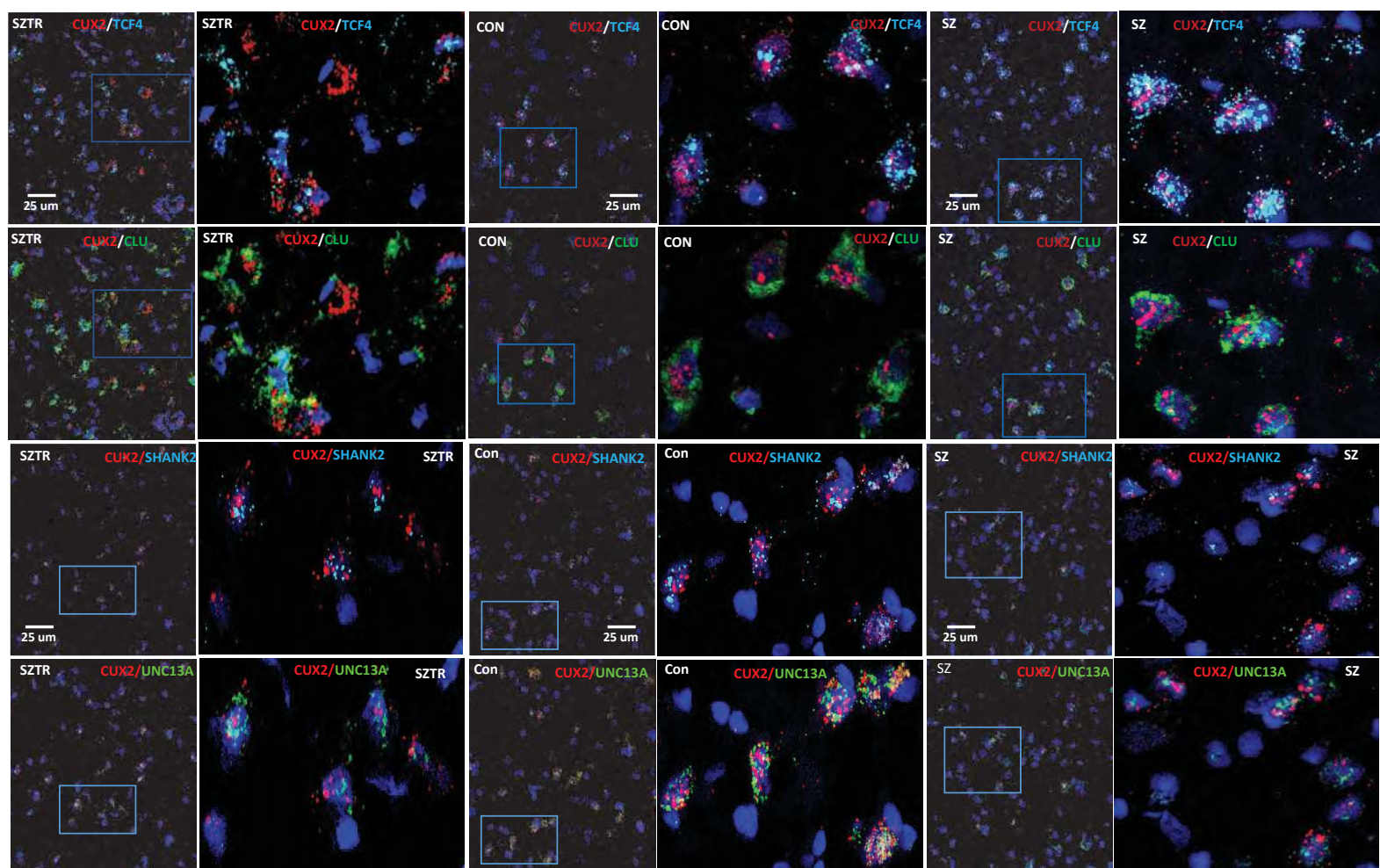
Extended Data Fig. 3. Rank rank hypergeometric overlap plot of cell-type-specific transcriptomic changes. Rank-Rank Hypergeometric Overlap plot depicting the similarity of transcriptional perturbations between all pairs of cell-types/states.

Classification  SZTR  CON  SZ
> 1%



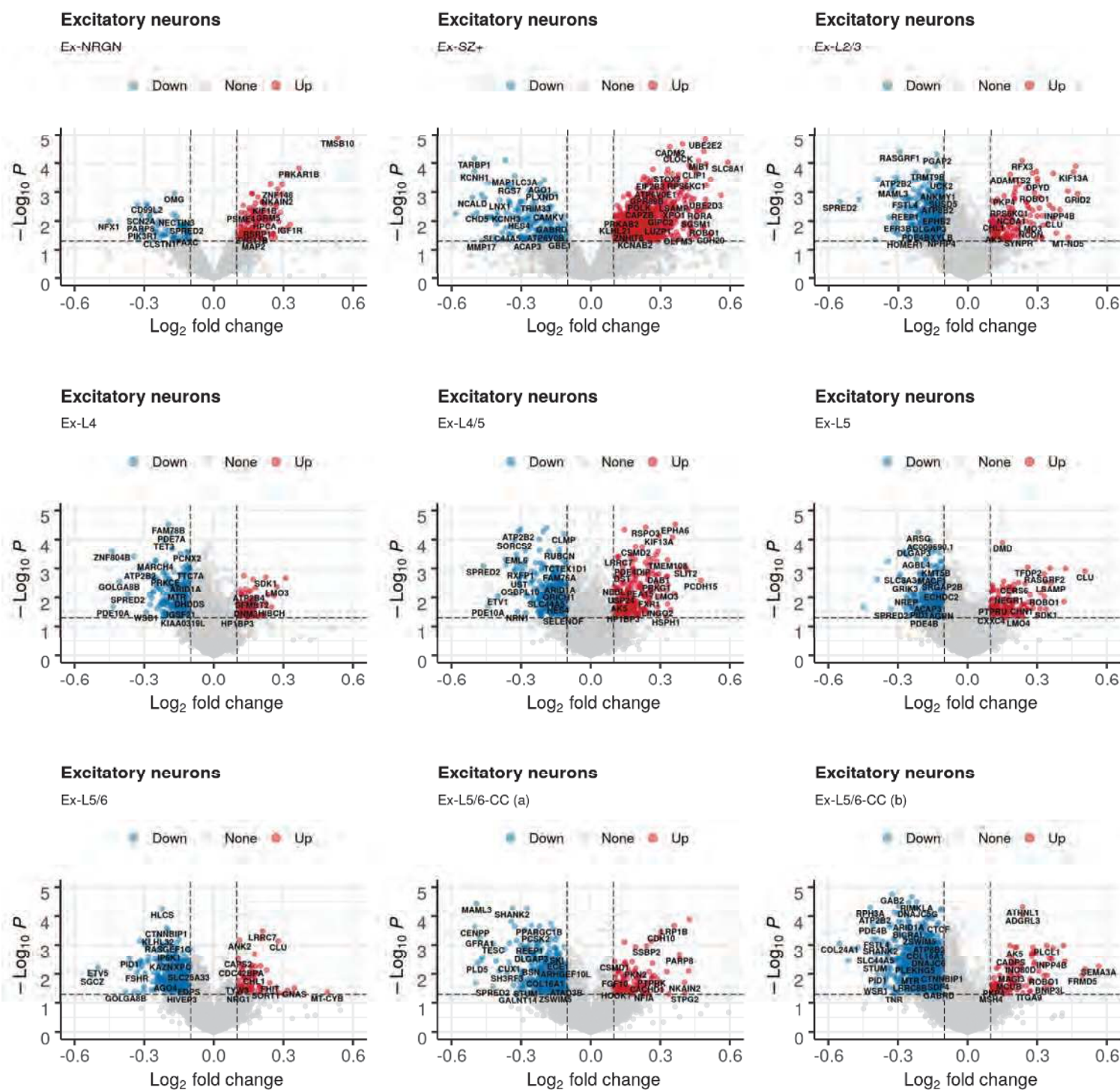
Extended Data Figure 4. Transcriptional pathology scores across subject classification. Transcriptional pathology scores across all individuals demonstrate clear gradation across classifications, with SZTR individuals (Ex-SZTR cell fraction > 1%) ranking below the majority of CON individuals, away from the SZ group.

Extended Data Figure 5. Fluorescence *in situ* hybridization of selected SZ DEGs



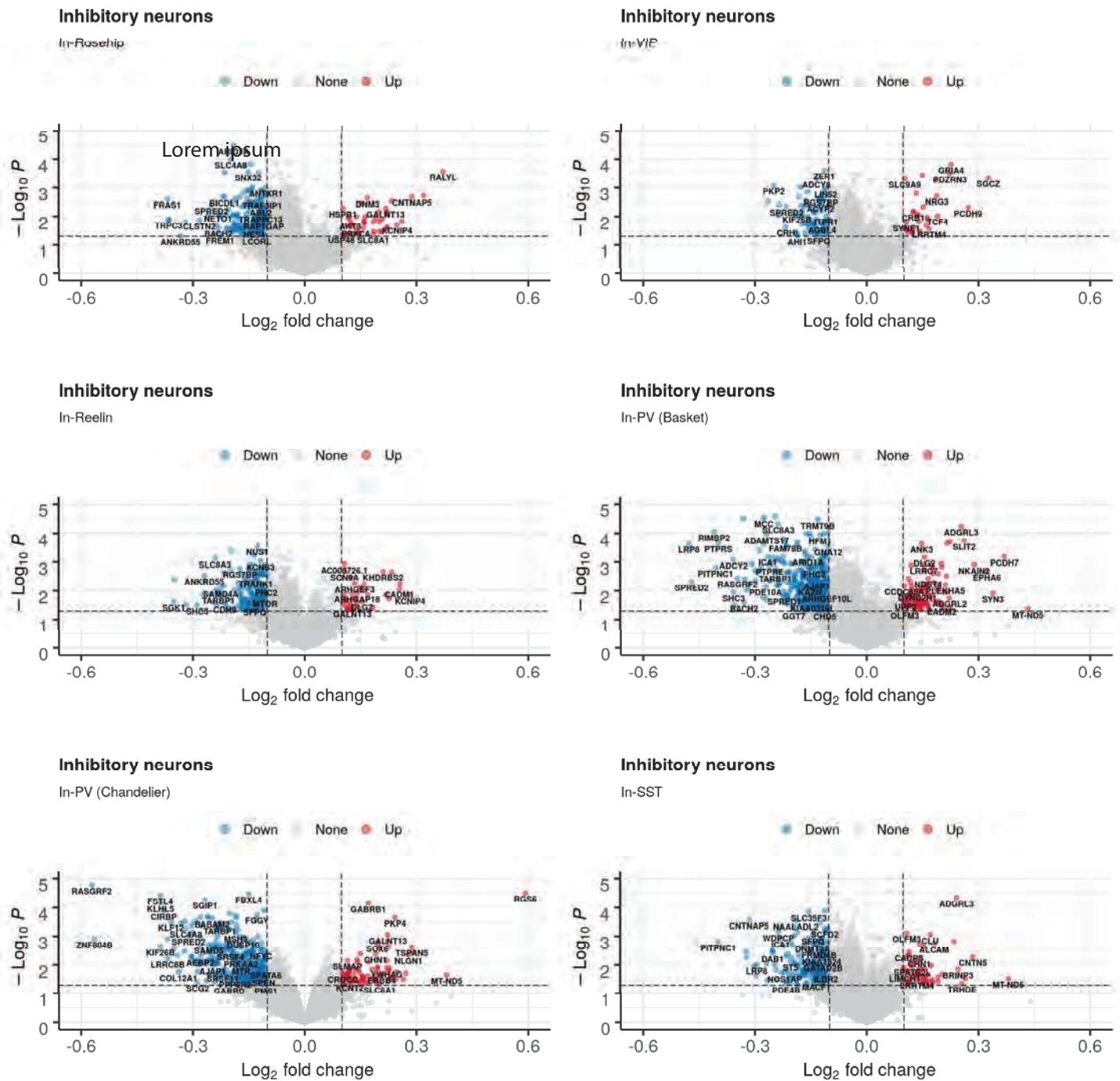
Extended Data Fig. 5 Fluorescence *in situ* hybridization of selected SZ DEGs. Representative photomicrographs from one case in each phenotype (SZTR, CON, SZ) are shown of *in situ* hybridization for the *CUX2* (Red, layer II and III excitatory neuron marker), *TCF4* (top, blue), *CLU* (middle, green), *SHANK2* (middle, blue), and *UNC13A* genes (bottom, green). Each image was captured at 40x magnification and for each image the full field of view is shown to the left, and the area boxed in blue is shown to the right. Each gene was assessed in two cases from each phenotype for six total cases.

Extended Data Figure 6a: volcano plots of SZ GWAS significance versus cell-type-specific transcriptional perturbation in excitatory neuronal populations



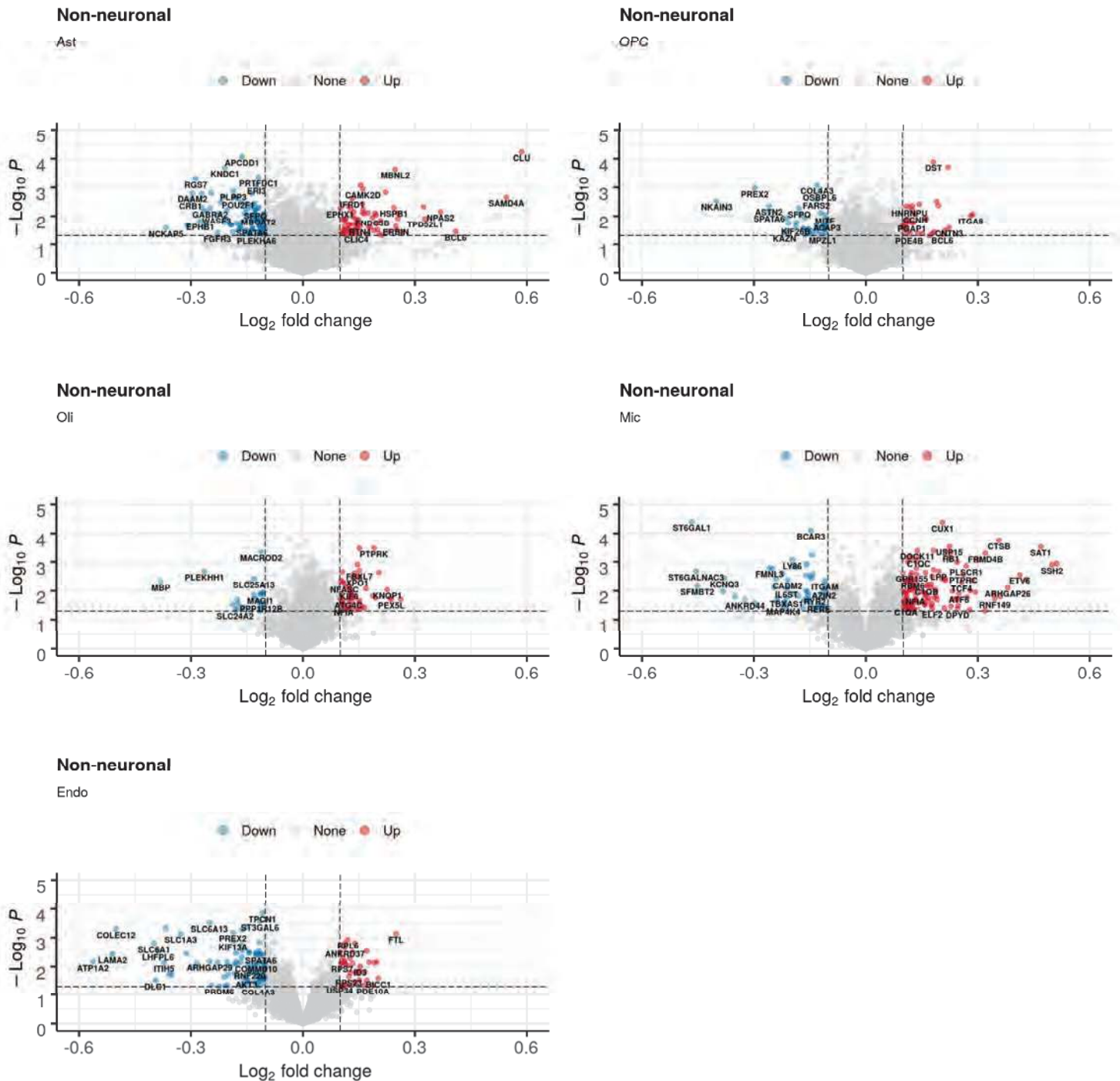
Extended Data Fig. 6a Genetic versus transcriptional SZ-associated perturbations. Volcano plots showing the relationship between SZ GWAS scores¹⁸ (y-axis, $-\log_{10}$ association p-value) and SZ transcriptional perturbations measured and reported herein (x-axis, \log_2 fold change of expression values in SZ relative to control samples). Plots are shown independently for subpopulations of excitatory neurons.

Extended Data Figure 6b Volcano plots of SZ GWAS significance versus cell-type-specific transcriptional perturbation in inhibitory neuronal populations



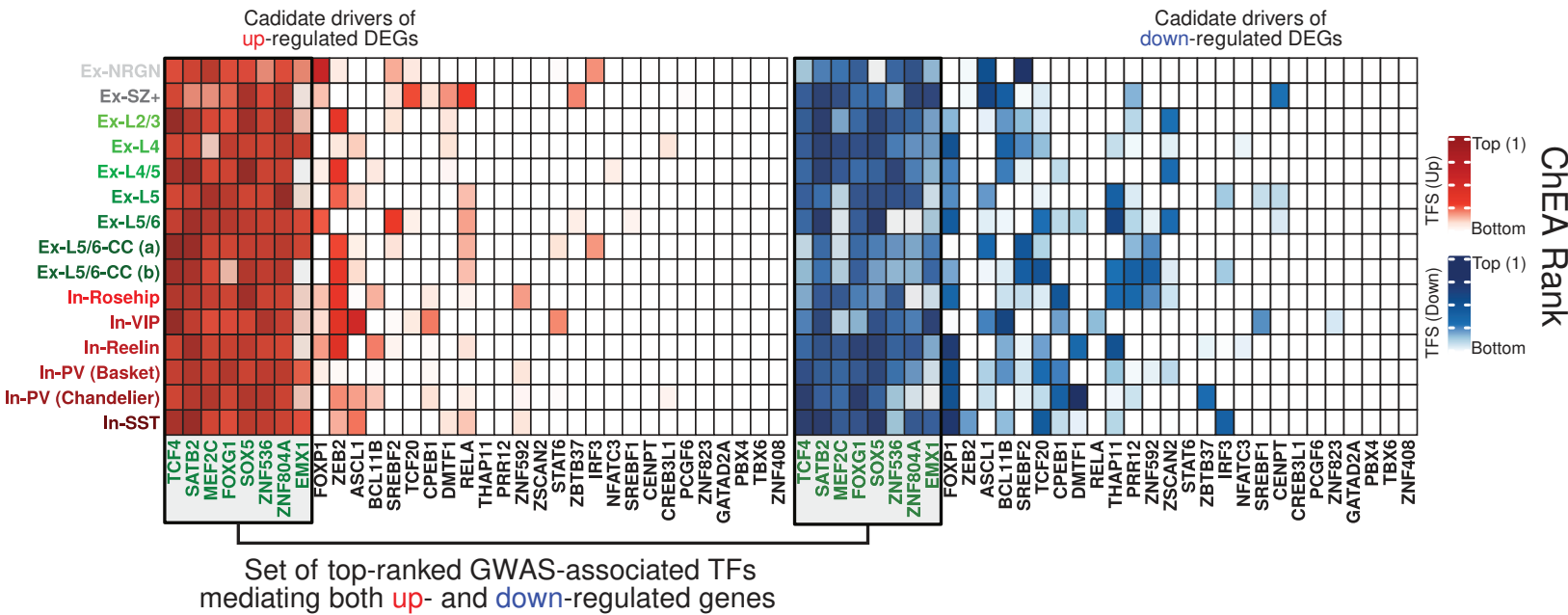
Extended Data Fig. 6b Genetic versus transcriptional SZ-associated perturbations. Volcano plots showing the relationship between SZ GWAS scores¹⁸ (y-axis, $-\log_{10}$ association p-value) and SZ transcriptional perturbations measured and reported herein (x-axis, \log_2 fold change of expression values in SZ relative to control samples). Plots are shown independently for subpopulations of inhibitory neuron subpopulations.

Extended Data Figure 6c: Volcano plots of SZ GWAS significance versus cell-type-specific transcriptional perturbation in non-neuronal populations

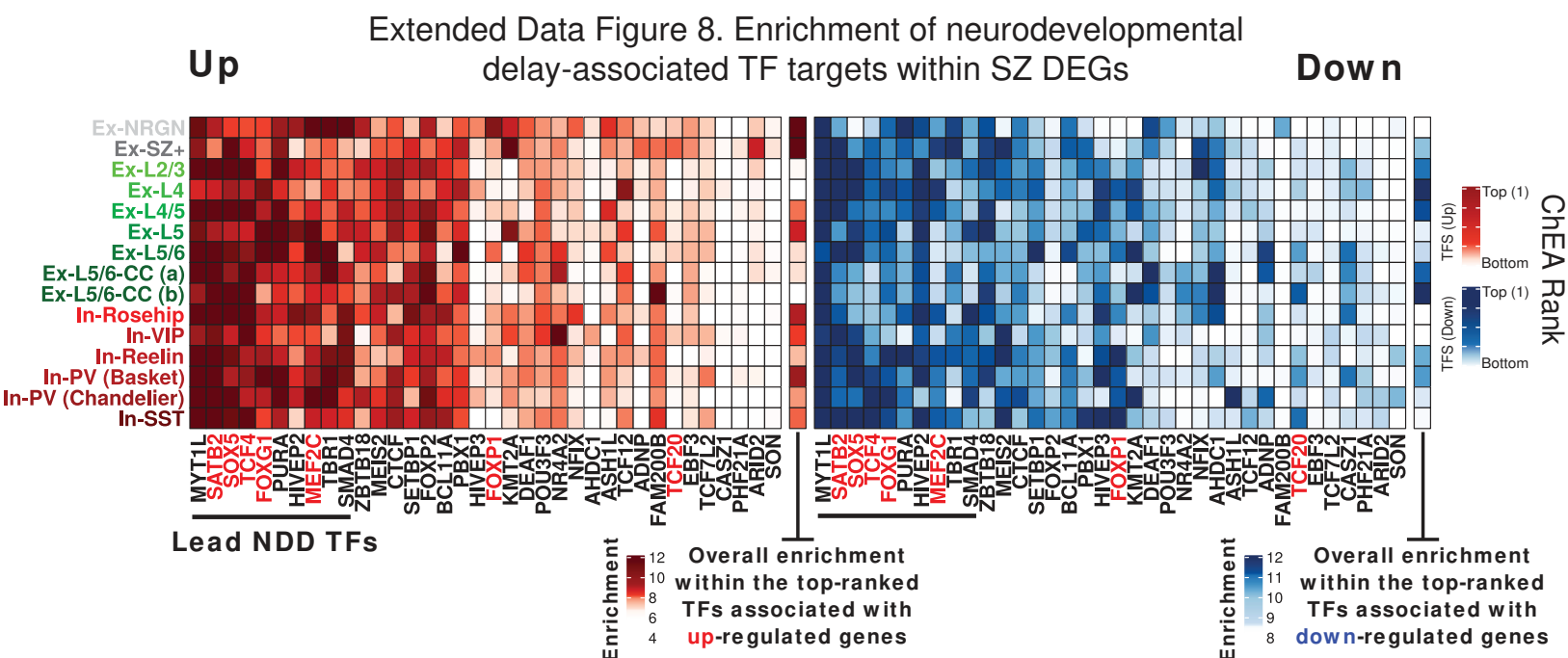


Extended Data Fig. 6c Genetic versus transcriptional SZ-associated perturbations. Volcano plots showing the relationship between SZ GWAS scores¹⁸ (y-axis, $-\log_{10}$ association p-value) and SZ transcriptional perturbations measured and reported herein (x-axis, \log_2 fold change of expression values in SZ relative to control samples). Plots are shown independently for subpopulations of non-neuronal subpopulations.

Extended Data Figure 7. Enrichment of SZ GWAS TF targets within SZ DEGs



Extended Data Fig. 7. Enrichment of SZ GWAS TF targets within SZ DEGs. Overrepresentation analysis (hypergeometric test) within targets of TFs genetically associated with SZ in GWAS (columns) of genes detected as differentially expressed in SZ relative to controls (rows). Overrepresentation analysis was performed independently for SZ upregulated (left) and downregulated genes (right).

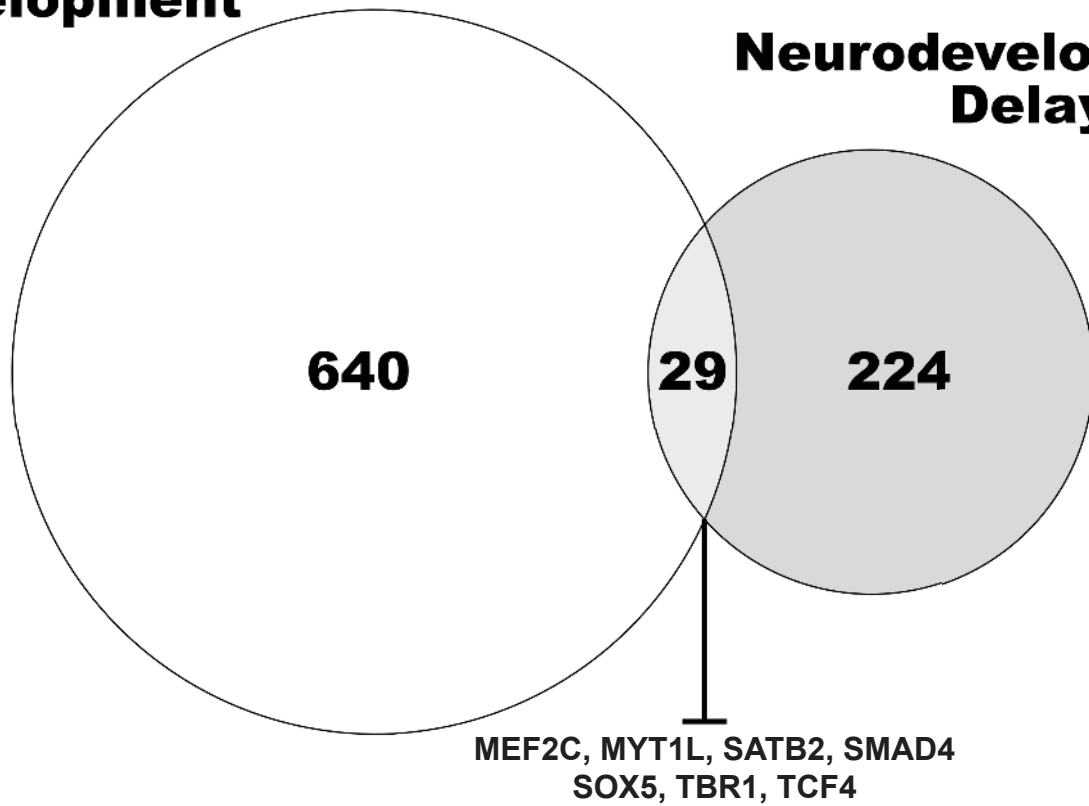


Extended Data Fig. 8 Enrichment of neurodevelopmental delay-associated TF targets within SZ DEGs. Overrepresentation analysis (hypergeometric test) within targets of TFs genetically associated with neurodevelopmental delay⁶⁵ (de novo mutations and CNVs) (columns) of genes detected as differentially expressed in SZ relative to controls (rows). Overrepresentation analysis was performed independently for SZ upregulated (left) and downregulated genes (right).

Extended Data Figure 9. Neurodevelopment and neurodevelopmental delay associated genes overlap

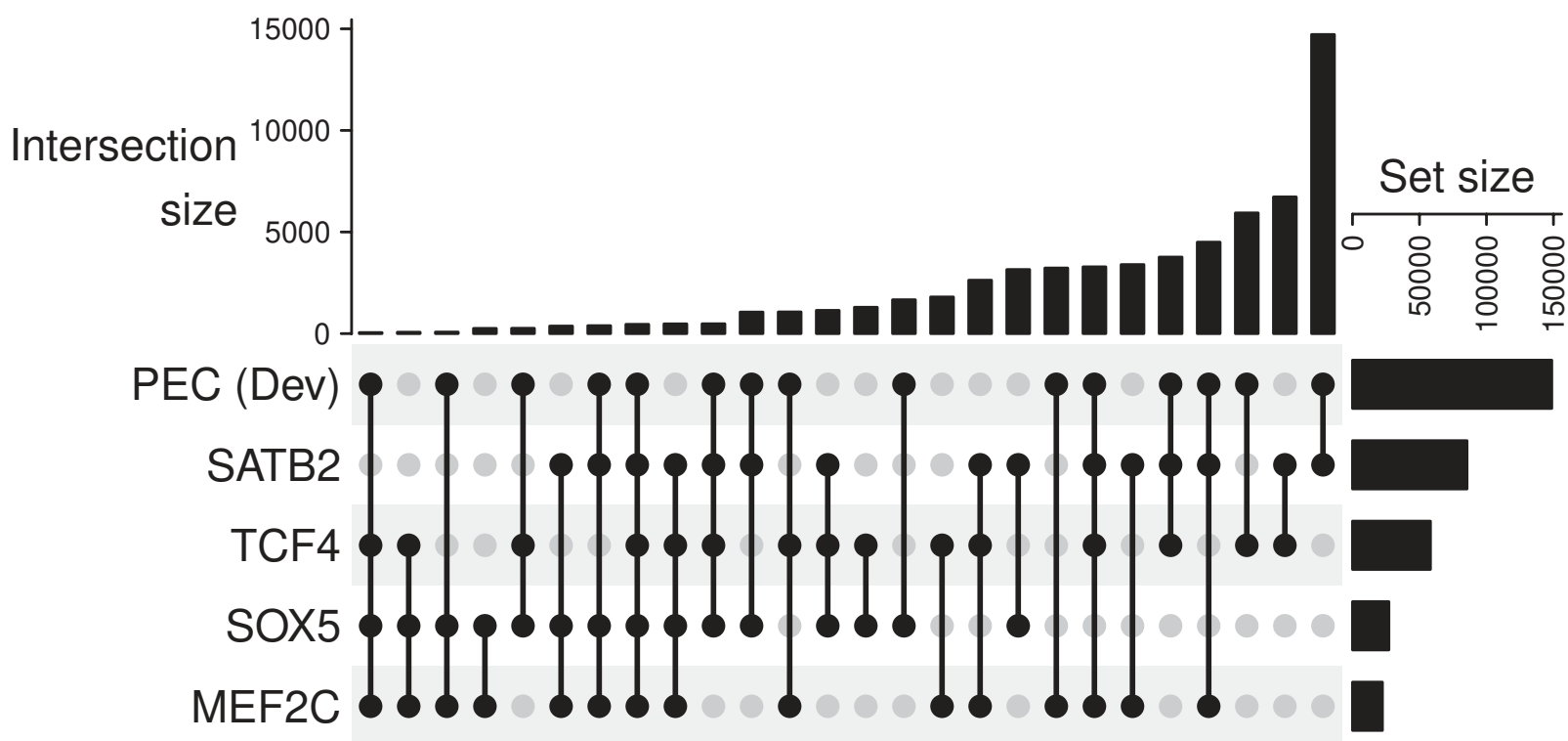
Neurodevelopment

Neurodevelopmental Delay



Extended Data Fig. 9 Neurodevelopment and neurodevelopmental delay associated genes overlap. Overlap of genes genetically associated with neurodevelopmental delay (NDD) and genes functionally annotated as related with neurodevelopment. SZ TFs are associated with both genesets. The majority of the lead NDD TFs (7/10) are also involved in neurodevelopment.

Extended Data Figure 10. Overlap of PEC developing human brain regulatory elements and observed TF binding sites in neuronal nuclei



Extended Data Fig. 10. Overlap of PEC developing human brain regulatory elements and observed TF binding sites in neuronal nuclei. The overlap of the total number of peaks for each transcription factor, defined as the union of top 1% peaks observed in any of the samples, with the masterset of PEC developing human brain dataset, containing H3K27Ac peaks for human brain samples at different stages of development.

References

1. Kahn, R. S. *et al.* Schizophrenia. *Nat Rev Dis Primers* **1**, 15067 (2015).
2. Forsyth, J. K. & Lewis, D. A. Mapping the Consequences of Impaired Synaptic Plasticity in Schizophrenia through Development: An Integrative Model for Diverse Clinical Features. *Trends Cogn. Sci.* **21**, 760–778 (2017).
3. Weinberger, D. R. On the plausibility of ‘the neurodevelopmental hypothesis’ of schizophrenia. *Neuropsychopharmacology* **14**, 1S–11S (1996).
4. Weinberger, D. R. Future of Days Past: Neurodevelopment and Schizophrenia. *Schizophr. Bull.* **43**, 1164–1168 (2017).
5. Kahn, R. S. & Keefe, R. S. E. Schizophrenia is a cognitive illness: time for a change in focus. *JAMA Psychiatry* **70**, 1107–1112 (2013).
6. Touloupoulou, T. *et al.* Polygenic risk score increases schizophrenia liability through cognition-relevant pathways. *Brain* **142**, 471–485 (2019).
7. Glessner, J. T. *et al.* Strong synaptic transmission impact by copy number variations in schizophrenia. *Proc. Natl. Acad. Sci. U. S. A.* **107**, 10584–10589 (2010).
8. Schwarz, E., Izmailov, R., Liò, P. & Meyer-Lindenberg, A. Protein Interaction Networks Link Schizophrenia Risk Loci to Synaptic Function. *Schizophr. Bull.* **42**, 1334–1342 (2016).
9. Nanou, E. & Catterall, W. A. Calcium Channels, Synaptic Plasticity, and Neuropsychiatric Disease. *Neuron* **98**, 466–481 (2018).
10. Mäki-Marttunen, T. *et al.* Functional Effects of Schizophrenia-Linked Genetic Variants on Intrinsic Single-Neuron Excitability: A Modeling Study. *Biol Psychiatry Cogn Neurosci Neuroimaging* **1**, 49–59 (2016).
11. Cao, H., Zhou, H. & Cannon, T. D. Functional connectome-wide associations of schizophrenia polygenic risk. *Mol. Psychiatry* (2020) doi:10.1038/s41380-020-0699-3.
12. Sekar, A. *et al.* Schizophrenia risk from complex variation of complement component 4. *Nature* **530**, 177–183 (2016).
13. Schizophrenia Working Group of the Psychiatric Genomics Consortium. Biological insights from 108 schizophrenia-associated genetic loci. *Nature* **511**, 421–427 (2014).
14. Pardiñas, A. F. *et al.* Common schizophrenia alleles are enriched in mutation-intolerant genes and in regions under strong background selection. *Nat. Genet.* **50**, 381–389 (2018).
15. Skene, N. G. *et al.* Genetic identification of brain cell types underlying schizophrenia. *Nat. Genet.* **50**, 825–833 (2018).
16. Guidotti, A. *et al.* Decrease in reelin and glutamic acid decarboxylase67 (GAD67) expression in schizophrenia and bipolar disorder: a postmortem brain study. *Arch. Gen. Psychiatry* **57**, 1061–1069 (2000).
17. Akbarian, S. *et al.* Gene expression for glutamic acid decarboxylase is reduced without loss of neurons in prefrontal cortex of schizophrenics. *Arch. Gen. Psychiatry* **52**, 258–266 (1995).

- 727 18. Fromer, M. *et al.* Gene expression elucidates functional impact of polygenic risk for schizophrenia. *Nat.*
728 *Neurosci.* **19**, 1442–1453 (2016).
- 729 19. Gandal, M. J. *et al.* Transcriptome-wide isoform-level dysregulation in ASD, schizophrenia, and bipolar
730 disorder. *Science* **362**, (2018).
- 731 20. Zheng, G. X. Y. *et al.* Massively parallel digital transcriptional profiling of single cells. *Nat. Commun.* **8**,
732 14049 (2017).
- 733 21. Aldridge, S. & Teichmann, S. A. Single cell transcriptomics comes of age. *Nat. Commun.* **11**, 4307 (2020).
- 734 22. Mathys, H. *et al.* Single-cell transcriptomic analysis of Alzheimer’s disease. *Nature* **570**, 332–337 (2019).
- 735 23. Velmeshev, D. *et al.* Single-cell genomics identifies cell type-specific molecular changes in autism.
736 *Science* **364**, 685–689 (2019).
- 737 24. Nagy, C. *et al.* Single-nucleus transcriptomics of the prefrontal cortex in major depressive disorder
738 implicates oligodendrocyte precursor cells and excitatory neurons. *Nat. Neurosci.* (2020)
739 doi:10.1038/s41593-020-0621-y.
- 740 25. Schafflick, D. *et al.* Integrated single cell analysis of blood and cerebrospinal fluid leukocytes in multiple
741 sclerosis. *Nat. Commun.* **11**, 247 (2020).
- 742 26. Wang, D. *et al.* Comprehensive functional genomic resource and integrative model for the human brain.
743 *Science* **362**, (2018).
- 744 27. McGinnis, C. S. *et al.* MULTI-seq: sample multiplexing for single-cell RNA sequencing using lipid-tagged
745 indices. *Nat. Methods* **16**, 619–626 (2019).
- 746 28. Mohammadi, S., Davila-Velderrain, J. & Kellis, M. A multiresolution framework to characterize single-cell
747 state landscapes. doi:10.1101/746339.
- 748 29. Boldog, E. *et al.* Transcriptomic and morphophysiological evidence for a specialized human cortical
749 GABAergic cell type. *Nat. Neurosci.* **21**, 1185–1195 (2018).
- 750 30. Lim, L., Mi, D., Llorca, A. & Marín, O. Development and Functional Diversification of Cortical Interneurons.
751 *Neuron* **100**, 294–313 (2018).
- 752 31. Demars, F. *et al.* Dysregulation of peripheral expression of the YWHA genes during conversion to
753 psychosis. *Sci. Rep.* **10**, 9863 (2020).
- 754 32. Enwright, J. F., Iii *et al.* Transcriptome alterations of prefrontal cortical parvalbumin neurons in
755 schizophrenia. *Mol. Psychiatry* **23**, 1606–1613 (2018).
- 756 33. Rannals, M. D. *et al.* Psychiatric Risk Gene Transcription Factor 4 Regulates Intrinsic Excitability of
757 Prefrontal Neurons via Repression of SCN10a and KCNQ1. *Neuron* **90**, 43–55 (2016).
- 758 34. Doostparast Torshizi, A. *et al.* Deconvolution of transcriptional networks identifies TCF4 as a master
759 regulator in schizophrenia. *Sci Adv* **5**, eaau4139 (2019).
- 760 35. Jaffe, A. E. *et al.* Mapping DNA methylation across development, genotype and schizophrenia in the
761 human frontal cortex. *Nat. Neurosci.* **19**, 40–47 (2016).
- 762 36. Pietersen, C. Y. *et al.* Molecular profiles of pyramidal neurons in the superior temporal cortex in

- 763 schizophrenia. *J. Neurogenet.* **28**, 53–69 (2014).
- 764 37. Pietersen, C. Y. *et al.* Molecular profiles of parvalbumin-immunoreactive neurons in the superior temporal
765 cortex in schizophrenia. *J. Neurogenet.* **28**, 70–85 (2014).
- 766 38. Südhof, T. C. Neuroligins and neurexins link synaptic function to cognitive disease. *Nature* **455**, 903–911
767 (2008).
- 768 39. Guilmatre, A., Huguet, G., Delorme, R. & Bourgeron, T. The emerging role of SHANK genes in
769 neuropsychiatric disorders. *Dev. Neurobiol.* **74**, 113–122 (2014).
- 770 40. Maynard, K. R. *et al.* dotdotdot: an automated approach to quantify multiplex single molecule fluorescent
771 in situ hybridization (smFISH) images in complex tissues. *Nucleic Acids Res.* **48**, e66 (2020).
- 772 41. Berdenis van Berlekom, A. *et al.* Synapse Pathology in Schizophrenia: A Meta-analysis of Postsynaptic
773 Elements in Postmortem Brain Studies. *Schizophr. Bull.* **46**, 374–386 (2020).
- 774 42. Birnbaum, R. & Weinberger, D. R. Genetic insights into the neurodevelopmental origins of schizophrenia.
775 *Nat. Rev. Neurosci.* **18**, 727–740 (2017).
- 776 43. Föcking, M. *et al.* Proteomic and genomic evidence implicates the postsynaptic density in schizophrenia.
777 *Mol. Psychiatry* **20**, 424–432 (2015).
- 778 44. Kristiansen, L. V., Beneyto, M., Haroutunian, V. & Meador-Woodruff, J. H. Changes in NMDA receptor
779 subunits and interacting PSD proteins in dorsolateral prefrontal and anterior cingulate cortex indicate
780 abnormal regional expression in schizophrenia. *Mol. Psychiatry* **11**, 737–47, 705 (2006).
- 781 45. Moon, M.-S. & Gomez, T. M. Balanced Vav2 GEF activity regulates neurite outgrowth and branching in
782 vitro and in vivo. *Molecular and Cellular Neuroscience* vol. 44 118–128 (2010).
- 783 46. Pilpel, Y. & Segal, M. Rapid WAVE dynamics in dendritic spines of cultured hippocampal neurons is
784 mediated by actin polymerization. *J. Neurochem.* **95**, 1401–1410 (2005).
- 785 47. Fawcett, J. P. *et al.* Nck adaptor proteins control the organization of neuronal circuits important for
786 walking. *Proc. Natl. Acad. Sci. U. S. A.* **104**, 20973–20978 (2007).
- 787 48. Cullen, T. J. *et al.* Anomalies of asymmetry of pyramidal cell density and structure in dorsolateral
788 prefrontal cortex in schizophrenia. *Br. J. Psychiatry* **188**, 26–31 (2006).
- 789 49. Garey, L. J. *et al.* Reduced dendritic spine density on cerebral cortical pyramidal neurons in schizophrenia.
790 *Journal of Neurology, Neurosurgery & Psychiatry* vol. 65 446–453 (1998).
- 791 50. Wagstyl, K. *et al.* Multiple markers of cortical morphology reveal evidence of supragranular thinning in
792 schizophrenia. *Transl. Psychiatry* **6**, e780 (2016).
- 793 51. Guet-McCreight, A., Skinner, F. K. & Topolnik, L. Common Principles in Functional Organization of
794 VIP/Calretinin Cell-Driven Disinhibitory Circuits Across Cortical Areas. *Front. Neural Circuits* **14**, 32 (2020).
- 795 52. Sey, N. Y. A. *et al.* A computational tool (H-MAGMA) for improved prediction of brain-disorder risk genes
796 by incorporating brain chromatin interaction profiles. *Nat. Neurosci.* **23**, 583–593 (2020).
- 797 53. Howard, D. M. *et al.* Genome-wide meta-analysis of depression identifies 102 independent variants and
798 highlights the importance of the prefrontal brain regions. *Nat. Neurosci.* **22**, 343–352 (2019).

- 799 54. Stahl, E. A. *et al.* Genome-wide association study identifies 30 loci associated with bipolar disorder. *Nat.*
800 *Genet.* **51**, 793–803 (2019).
- 801 55. Grove, J. *et al.* Identification of common genetic risk variants for autism spectrum disorder. *Nat. Genet.* **51**,
802 431–444 (2019).
- 803 56. Demontis, D. *et al.* Discovery of the first genome-wide significant risk loci for attention deficit/hyperactivity
804 disorder. *Nat. Genet.* **51**, 63–75 (2019).
- 805 57. Jansen, I. E. *et al.* Genome-wide meta-analysis identifies new loci and functional pathways influencing
806 Alzheimer's disease risk. *Nat. Genet.* **51**, 404–413 (2019).
- 807 58. Cross-Disorder Group of the Psychiatric Genomics Consortium *et al.* Genetic relationship between five
808 psychiatric disorders estimated from genome-wide SNPs. *Nat. Genet.* **45**, 984–994 (2013).
- 809 59. Maynard, K. E., Collado-Torres, L., Weber, L. M. & Uyttingco, C. Transcriptome-scale spatial gene
810 expression in the human dorsolateral prefrontal cortex. *bioRxiv* (2020).
- 811 60. Metzner, C., Zurowski, B. & Steuber, V. The Role of Parvalbumin-positive Interneurons in Auditory Steady-
812 State Response Deficits in Schizophrenia. *Sci. Rep.* **9**, 18525 (2019).
- 813 61. Bartos, M., Vida, I. & Jonas, P. Synaptic mechanisms of synchronized gamma oscillations in inhibitory
814 interneuron networks. *Nat. Rev. Neurosci.* **8**, 45–56 (2007).
- 815 62. Forrest, M. P. *et al.* The Psychiatric Risk Gene Transcription Factor 4 (TCF4) Regulates
816 Neurodevelopmental Pathways Associated With Schizophrenia, Autism, and Intellectual Disability.
817 *Schizophr. Bull.* **44**, 1100–1110 (2018).
- 818 63. Larti, F. *et al.* A defect in the CLIP1 gene (CLIP-170) can cause autosomal recessive intellectual disability.
819 *Eur. J. Hum. Genet.* **23**, 416 (2015).
- 820 64. Liu, X., Li, Y. I. & Pritchard, J. K. Trans Effects on Gene Expression Can Drive Omnigenic Inheritance. *Cell*
821 **177**, 1022–1034.e6 (2019).
- 822 65. Keenan, A. B. *et al.* ChEA3: transcription factor enrichment analysis by orthogonal omics integration.
823 *Nucleic Acids Res.* **47**, W212–W224 (2019).
- 824 66. Lai, T. *et al.* SOX5 controls the sequential generation of distinct corticofugal neuron subtypes. *Neuron* **57**,
825 232–247 (2008).
- 826 67. Zahr, S. K., Kaplan, D. R. & Miller, F. D. Translating neural stem cells to neurons in the mammalian brain.
827 *Cell Death Differ.* **26**, 2495–2512 (2019).
- 828 68. Phillips, J. M. Neurodevelopmental and Genetic Disorders: A Book Review - Handbook of
829 Neurodevelopmental and Genetic Disorders in Children. Second edition, Sam Goldstein, Cecil R.
830 Reynolds (Eds.). (2011). New York: The Guilford Press, 588 pp., \$75.00 (HB). *Journal of the International*
831 *Neuropsychological Society* vol. 17 1167–1168 (2011).
- 832 69. Coe, B. P. *et al.* Neurodevelopmental disease genes implicated by de novo mutation and copy number
833 variation morbidity. *Nat. Genet.* **51**, 106–116 (2019).
- 834 70. Li, M. *et al.* Integrative functional genomic analysis of human brain development and neuropsychiatric

- 835 risks. *Science* **362**, (2018).
- 836 71. Kaya-Okur, H. S. *et al.* CUT&Tag for efficient epigenomic profiling of small samples and single cells. *Nat.*
837 *Commun.* **10**, 1930 (2019).
- 838 72. Harrington, A. J. *et al.* MEF2C regulates cortical inhibitory and excitatory synapses and behaviors relevant
839 to neurodevelopmental disorders. *Elife* **5**, (2016).
- 840 73. Verret, L. *et al.* Inhibitory interneuron deficit links altered network activity and cognitive dysfunction in
841 Alzheimer model. *Cell* **149**, 708–721 (2012).
- 842 74. Gonzalez-Burgos, G., Cho, R. Y. & Lewis, D. A. Alterations in cortical network oscillations and
843 parvalbumin neurons in schizophrenia. *Biol. Psychiatry* **77**, 1031–1040 (2015).
- 844 75. Nelson, M. R. *et al.* The support of human genetic evidence for approved drug indications. *Nat. Genet.* **47**,
845 856–860 (2015).
- 846 76. Butler, A., Hoffman, P., Smibert, P., Papalexi, E. & Satija, R. Integrating single-cell transcriptomic data
847 across different conditions, technologies, and species. *Nat. Biotechnol.* **36**, 411–420 (2018).
- 848 77. Mohammadi, S., Ravindra, V., Gleich, D. F. & Grama, A. A geometric approach to characterize the
849 functional identity of single cells. *Nat. Commun.* **9**, 1516 (2018).
- 850 78. Batagelj, V. *An $O(m)$ Algorithm for Cores Decomposition of Networks.* (2001).
- 851 79. Crowell, H. L. *et al.* On the discovery of population-specific state transitions from multi-sample multi-
852 condition single-cell RNA sequencing data. *bioRxiv* 713412 (2019) doi:10.1101/713412.
- 853 80. Ritchie, M. E. *et al.* limma powers differential expression analyses for RNA-sequencing and microarray
854 studies. *Nucleic Acids Res.* **43**, e47 (2015).
- 855 81. Law, C. W., Chen, Y., Shi, W. & Smyth, G. K. voom: Precision weights unlock linear model analysis tools
856 for RNA-seq read counts. *Genome Biol.* **15**, R29 (2014).
- 857 82. Meers, M. P., Tenenbaum, D. & Henikoff, S. Peak calling by Sparse Enrichment Analysis for CUT&RUN
858 chromatin profiling. *Epigenetics Chromatin* **12**, 42 (2019).
- 859 83. He, Z. *et al.* Comprehensive transcriptome analysis of neocortical layers in humans, chimpanzees and
860 macaques. *Nat. Neurosci.* **20**, 886–895 (2017).

861

862